Nutrigenomic Regulation of Sensory Plasticity

Hayeon Sung[1#], Anoumid Vaziri[1, 2, #], Daniel Wilinski[1], Riley K.R. Woerner[1], Peter L. Freddolino[3, 4], Monica Dus[1, 2, 5 *]

[1] Department of Molecular, Cellular and Developmental Biology, College of Literature, Science, and the Arts, The University of Michigan, Ann Arbor, MI 49109

[2] The Molecular, Cellular and Developmental Biology Graduate Program, The University of Michigan, Ann Arbor, MI 49109

[3] Department of Biological Chemistry, The University of Michigan Medical School, Ann Arbor, MI 48109, USA

[4] Department of Computational Medicine and Bioinformatics, The University of Michigan Medical School, Ann Arbor, MI 48109, USA

[5] The Michigan Neuroscience Institute, Ann Arbor, MI 48109, USA

# equal contribution

* Correspondence: mdus@umich.edu

Keywords

Nutriepigenetics, Nutrigenomics, sweet taste plasticity, sensory adaptations.

Abstract

Diet profoundly influences brain physiology, but how nutritional information is transmuted into neural activity and behavior changes remains elusive. Here we show that the metabolic enzyme O-GlcNAc Transferase (OGT) moonlights on the chromatin of the *D. melanogaster* gustatory neurons to instruct changes in chromatin accessibility and transcription that underlie sensory adaptations to a high sugar diet. OGT works synergistically with the Mitogen Activated Kinase/Extracellular signal Regulated Kinase (MAPK/ERK) *rolled* and its effector *stripe* (also known as EGR2 or Krox20) to integrate activity information. OGT also cooperates with the epigenetic silencer *Polycomb Repressive Complex 2.1* (PRC2.1) to decrease chromatin accessibility and repress transcription in the high sugar diet. This integration of nutritional and activity information changes the taste neurons' responses to sugar and flies' ability to sense sweetness. Our findings reveal how nutrigenomic signaling generates cell-specific responses to global nutrient variations.

INTRODUCTION

The levels and types of dietary nutrients play an essential role in cellular processes such as growth, division, and differentiation by providing fuel and biomass. However, nutrients can also affect these aspects of cell physiology by influencing, and often orchestrating, gene expression programs (Dai et al., 2020; Vaziri and Dus, 2021). These effects are mediated through nutrient-sensitive modifications to DNA, RNA, and proteins, as well as changes to the activity, binding, and localization of enzymes and signaling factors (Huang et al., 2015; Katada et al., 2012). These nutrigenomic signaling pathways –nutrigenomics is the field that studies food-genes interactions– could explain how the food environment affects the risk of non-communicable diseases such as diabetes, cancer, and neurodegeneration. They also hold the potential to uncover new interventions and treatments for these debilitating diseases. While the effects of nutrients on gene expression are well-established, relatively little is known about the molecular mechanisms at the food-gene interface. A significant challenge of the field has been to explain how global variations in the nutrient environment lead to specific changes in cell physiology. To overcome these challenges, we have developed an experimental system where the contributions of nutrients to physiology can be studied mechanistically and *in vivo (Vaziri and Dus, 2021)*. Here we use this model to characterize how cell-specific signals are integrated with broad changes in metabolism to drive adaptations to the dietary environment.

Taste sensation changes depending on diet composition. In animals, the levels of bitter, sweet, and salty foods influence how these taste stimuli are perceived, with a general inverse relationship between the amount of a particular food in the diet and the responses of the sensory system to it (May and Dus, 2021; Reed et al., 2020; Sarangi and Dus, 2021). For example, in humans and rodents, the dietary concentration of sugars affects sweetness intensity or the electrophysiological responses of the sensory nerves to sucrose (May and Dus, 2021; McCluskey et al., 2020; Sartor et al., 2011; Sung et al., 2022; Wise et al., 2016). A similar phenomenon occurs in flies, where diets supplemented with 15-30% sucrose, glucose, or fructose decrease the responses of the sensory neurons to sucrose and the transmission of the sweetness signal to higher brain areas (May et al. 2019; Vaziri et al. 2020; Wang et al. 2020; Ganguly et al. 2021; May et al. 2020). In rats and flies, the dulling of the sensory system to sugar occurs even without weight gain, suggesting that diet exposure is sufficient to drive sweet taste plasticity (Sung et al. 2022; May et al. 2019). Our previous work in flies implicated metabolic signaling through the Hexosamine Biosynthesis Pathway (HBP) enzyme O-GlcNaC Transferase (OGT) in this phenomenon (May et al., 2019). Specifically, knockdown of OGT exclusively in the fly sweet-taste

cells prevented the neural and behavioral decrease in sugar responses observed with a high-sugar diet (May et al., 2019). OGT uses the metabolic end-product of the HBP, UDP-GlcNAc, to post-translationally modify proteins and change their stability or activity (Hart, 2019). OGT activity is sensitive to all cellular levels of UDP-GlcNAc without substrate inhibition, but it is enhanced by high dietary sugar due to a higher flux through the HBP (Bouché et al., 2004; Hanover et al., 2010; Hawkins et al., 1997; Marshall et al., 2004; May et al., 2019; Na et al., 2015; Olivier-Van Stichelen et al., 2017; Wang et al., 1998; Wilinski et al., 2019). OGT is also a nucleocytoplasmic protein that interacts with many chromatin- and DNA-modifying complexes; as such, it is thought to function as a nutrigenomic sensor, bridging diet and genes (Hardivillé and Hart, 2014; Hart, 2019; Olivier-Van Stichelen et al., 2017; Olivier-Van Stichelen and Hanover, 2015). Despite global changes in HBP flux with high dietary sugar, the consequences of OGT activity differ among cell types. Understanding how this occurs would provide an opportunity to uncover how specificity is achieved in nutrigenomic signaling. Here we exploited the effects of OGT on *Drosophila* sensory neurons and the exquisite genetic tools of this organism to investigate this question. Our experiments reveal that nutrigenomic specificity is achieved through integrating metabolic state with cell-specific experience. In the sensory neurons, OGT decorates nutrient-sensitive loci also occupied by the epigenetic silencer *PRC2.1* and the activity-dependent ERK effector Stripe (*Sr*). This cooperation leads to changes in chromatin accessibility and transcription that drive sensory plasticity, and the catalytic activity of OGT plays an instructional role in this process. Thus, our results uncover mechanistic insights into how nutrigenomic signaling translates nutritional information into cell-specific adaptations.

RESULTS

The nutrient sensor OGT decorates the chromatin of sweet sensory cells.

Since transcriptional changes have been implicated in sugar diet-induced taste plasticity (May et al., 2019; Vaziri et al., 2020; Wang et al., 2020) and OGT associates with chromatin binding factors (Gambetta and Müller, 2015; Gao et al., 2018; Hart et al., 2011; Vella et al., 2013), we asked whether this metabolic enzyme moonlights on the chromatin of sweet taste neurons. We used DNA adenosine methyltransferase Identification (Dam-ID or TaDA) to measure the association of OGT with DNA (Marshall et al., 2016; van Steensel and Henikoff, 2000) and Chromatin Accessibility profiling using Targeted DamID (CaTaDA) to assess chromatin accessibility (Sen et al., 2019). Transgenic UAS-*LT3-Dam::OGT* or UAS-LT3-*Dam* flies were

98 crossed with *Gustatory Receptor 5a* GAL4 (*Gr5a*) flies (Chyb et al., 2003) to drive expression
99 exclusively in the ~60 sweet taste cells of the fly mouthpart, and *Tubulin-GAL80ts* to control the
100 timing of transgene induction. *Gr5a>LT3-Dam::OGT; tubulin-GAL80ts* (green) and *Gr5a>LT3-*
101 *Dam; tubulin-GAL80ts* (yellow) transgenic flies were kept at the permissive temperature and fed
102 a control (CD, 5% sucrose) or sugar (SD, 30% sucrose) diet for 3 days. *Dam::OGT* and *Dam* were
103 then induced by heat shocking the animals at 30°C for 18 hours on day 4, as in our prior
104 experimental design (Fig. 1A) (Vaziri et al., 2020). The normalized *Dam::OGT* replicates clustered
105 together by diet (Fig. S1A), and the chromatin accessibility profile of Dam at the *Gr5a* sweet taste
106 receptor gene promoter was high, while at the bitter *Gustatory Receptor Gr66a* promoter– only
107 expressed in adjacent cells– accessibility was low (Fig. S1B), suggesting that these transgenes
108 were targeted to the correct cells.

109 Dam::OGT was associated with chromatin at introns (51%) and Transcriptional Start Sites
110 (TSS) and promoters (30%) (Fig. 1B, Supplemental File 1); these patterns are similar to those
111 observed in the only other study that measured OGT occupancy on the chromatin of mouse
112 embryonic stem cells (Vella et al., 2013). In flies, chromatin types are classified according to the
113 histone modifications present and the proteins bound (Filion et al., 2010). Using this chromatin
114 characterization, we found that OGT was enriched in transcriptionally active euchromatin,
115 characterized by H3K4 and H3K36 methylation (also known as “yellow”) (Fig. 1C). OGT was also
116 enriched at “blue” Polycomb heterochromatin decorated by H3K27 methylation and bound by
117 PRC2 (Fig. 1C) (Filion et al., 2010; Vaziri et al., 2020).

118 We next examined the differential binding of OGT between the two diets. Although the
119 majority of intervals were shared between a CD and SD (Fig. 1D, find_peaks FDR <0.01), a few
120 hundred loci were uniquely associated with OGT in either the CD (36%) or SD (10%) condition.
121 However, the chromatin accessibility at OGT-bound peaks decreased in the high sugar diet
122 condition (Fig. 1E). To characterize the function of the genes occupied by OGT, we performed
123 pathway enrichment analysis using iPAGE (Goodarzi et al., 2009). On CD, OGT-decorated genes
124 were involved in signal transduction, membrane potential, and calmodulin-dependent protein
125 kinase activity (Fig. 1F, left). Instead, genes targeted by OGT in the SD condition were enriched
126 in G-protein coupled receptor activity, synaptic target attraction, and transcription (Fig. 1F, left).
127 Finally, genes with differential OGT binding were enriched for regulatory/signaling and neural GO
128 terms, including dendrite morphogenesis, neuron projection membrane, synaptic target attraction,
129 signal transduction, pattern formation, and asymmetric cell division (Fig. 1F right, for full iPAGE,
130 GO term analysis see Fig. S2). Together, these experiments show that OGT resides on the

131 chromatin of the sweet taste at open domains characterized by a small, but significant diet
132 sensitivity, and that genes associated with neural functions are particularly abundant among the
133 set with diet-dependent OGT binding.

134

135 **OGT and PRC2.1 share diet-sensitive chromatin sites.**

136 Our previous work showed that the epigenetic silencer PRC2.1– specifically its histone 3
137 lysine 27 methyltransferase activity– was necessary and sufficient to drive sweet taste plasticity
138 in response to the nutrient environment (Vaziri et al., 2020). In the presence of high dietary sugar,
139 PRC2.1 decreased chromatin accessibility and expression of transcription factors involved in
140 synaptic function and signaling. Silencing these genes and their regulons lowered neural and
141 behavioral responses to sweetness in high-sugar diet flies (Vaziri et al., 2020). Since OGT and
142 PRC2.1 play a role in sweet taste plasticity and OGT occupancy was enriched at blue Polycomb
143 chromatin, we asked whether there was an overlap in their occupancy.

144 A comparison of the peaks occupied by both *Dam::Pcl* (*pink*, *Pcl* is the recruiter for
145 PRC2.1) and *Dam::OGT* (green) revealed a small number of shared intervals (Fig. 2A, ~10%;
146 Supplemental File 1). These 162 loci were enriched in the blue "Polycomb" chromatin ($p<0.001$,
147 permutation test) and had lower expression levels in the *Gr5a*+ neurons (from TRAP experiment
148 in (Vaziri et al., 2020)) compared to those bound by OGT alone (Fig. 2B, *purple* vs. *green*) (Fig.
149 1C) (Filion et al., 2010). OGT x Pcl intervals had higher expression than those occupied by
150 PRC2.1 alone, suggesting they may represent a subtype of Polycomb chromatin (Fig. 2B, *purple*
151 vs. *pink*). We next asked whether the dietary environment changed the association of OGT and
152 Pcl at these loci. There was more OGT and Pcl at the OGT x Pcl shared sites in the SD condition
153 compared to CD, and more OGT than Pcl was present at these sites in both diets (Fig. 2C).
154 Strikingly, chromatin accessibility at OGT x Pcl was markedly (50%) decreased on SD compared
155 to CD (Fig. 2D). This nutrient-dependent shift in accessibility was 3-fold higher at the shared loci
156 compared to those bound by OGT alone (compare Figs. 1E and 2D; also comparatively higher
157 than those bound by PRC2.1 alone (Vaziri et al., 2020)).

158 GO term analysis of genes shared by OGT/Pcl targets revealed enrichment in regulatory
159 pathways involved in sequence-specific DNA binding, including those implicated in neural
160 differentiation, sodium channel regulator activity, Activin receptor signaling, and dendrite
161 development (Fig. 2E, left). 30% of the OGT x Pcl sites corresponded to genes encoding DNA-

binding and regulatory factors, including two Homeobox transcription factors known to play a role in sweet taste function and plasticity, *cad* and *Ptx1* (Fig. 2E, right) (Vaziri et al., 2020). Analysis of protein interactions between OGT x PRC2.1 genes (Szklarczyk et al., 2020) uncovered a Protein-Protein Interaction network enrichment (*p<1.0e-16*) among DNA-binding factors (pink, *p=2.08e-09*), Mitogen-Activated Protein Kinase (MAPK, blue, *p=0.00059*), signal transduction (Tumor Growth Factor TGF-β/Activin signaling, yellow), neuron projection (red outline, *p=4.95e-7*), and response to stimuli (p=7.15e-0.5). Interestingly, the MAPK pathway is sensitive to neural activity and nutrients (Papa et al., 2019; Robles-Flores et al., 2021).

The catalytic activity of OGT is required for all aspects of diet-induced taste plasticity.

Our data show that OGT moonlights on the chromatin of the sensory neurons and that its binding is diet-dependent at loci also occupied by PRC2.1. To understand the effects of OGT function, and thus nutrigenomic signaling, on taste plasticity, we inhibited the catalytic activity of OGT using the OGT Small Molecule Inhibitor-1 (OSMI) (May et al., 2020; Ortiz-Meoz et al., 2015)(Fig. 3A). Although OSMI treatment is not specific to sweet taste cells, this approach has several advantages: 1) it only affects the catalytic activity of OGT, not its protein levels; 2) it allows us to manipulate OGT activity only during the dietary exposure period, and 3) it makes experiments that would be otherwise inaccessible because of complex genetic combinations and lethality possible.

We first tested the effects of OGT inhibition on taste plasticity by feeding flies a CD or SD supplemented with 10uM of OSMI or vehicle (DMSO) and conducted the Proboscis Extension Response (PER) assay, which measures taste responses. In this assay, the fly proboscis–which houses the dendrites of the sensory neurons (Fig. 3B)– is stimulated with different concentrations of sucrose. The amount of proboscis extension is measured to generate a taste intensity curve (Fig. 3C). Flies on CD had high PER to both low (5%) and high (30%) sucrose concentrations, that decreased with consumption of a high sugar diet for 7 days (Fig. 3C, left). Inhibition of OGT activity, however, resulted in the same taste responses on both diets (Fig. 3C, right). This effect of OSMI on taste plasticity was identical to that observed with knockdown of OGT in the Gr5a+ neurons (Fig. S3A, green; knockdown efficiency is 50%), suggesting that OGT activity plays an essential role in taste plasticity.

192 We used this experimental design to then ask how OGT activity affected chromatin
193 accessibility and PRC2.1 binding at OGT x Pcl co-occupied loci in response to diet (Fig. 3A). To
194 do this, we fed *Gr5a>LT3-Dam; tubulin-GAL80* (Fig. 3A) and *Gr5a>LT3-Dam::Pcl; tubulin-Gal80ts*
195 (Fig. S4A) flies a CD or a SD supplemented with OSMI. Strikingly, OSMI treatment completely
196 abolished the changes in chromatin accessibility observed with SD at OGT x Pcl sites (Fig. 3D,
197 compared to Fig. 2D; Supplemental File 1), suggesting that OGT activity is necessary for diet-
198 dependent dynamics at these loci. However, inhibition of OGT activity did not affect Pcl occupancy
199 at these peaks, indicating that recruitment of PRC2.1 to these sites is largely independent of this
200 metabolic enzyme. OSMI also had a mild effect on the occupancy of *Dam::Pcl* genomewide since
201 the number (~1800) and identity (80%) of Dam::Pcl peaks were mainly the same with or without
202 OSMI (Fig. S4C and Fig. S5). Only a smaller fraction of new PRC2.1-only peaks emerged with
203 OSMI treatment (Fig. S4C), and the genes in these intervals were enriched in GO terms such as
204 detection of chemical stimuli, DNA binding, and protein kinase activation (Fig. S5). Thus, OGT
205 activity is required for the diet-dependent decrease in chromatin accessibility but not PRC2.1
206 recruitment or occupancy. Notably, the catalytic activity of OGT was also necessary for PRC2.1-
207 mediated taste modulation. Overexpression of *Pcl* in the Gr5a+ neurons mimics the effects of SD
208 on taste by decreasing responses to sucrose in flies fed a CD (Fig. 3E, *left*)– a result dependent
209 on the H3K27 methylation activity of this complex (Vaziri et al., 2020). However, OSMI blocked
210 the effects of *Pcl* overexpression on sucrose responses compared to vehicle-fed flies (Fig. 3E,
211 *right*). These results argue for a strong genetic interaction between OGT and PRC2.1 and place
212 this metabolic enzyme upstream of PRC2.1 at both the molecular and behavioral levels.

213 To understand the consequences of the observed OGT-dependent shifts in chromatin
214 accessibility, we isolated mRNAs associated with the ribosomes of the *Gr5a*+ cells using
215 Translating mRNA Affinity Purification (TRAP) (Chen and Dickman, 2017) in flies fed a CD+OSMI
216 and SD +OSMI. Principal component analysis revealed that most of the variation between
217 samples was due to diet (Fig. S6A); mRNAs specifically expressed in the *Gr5a*+ cells, such as
218 the sweet taste receptor genes (*Gr5a*, *Gr64f*, and *Gr64a)* and the fatty acids taste receptor *Ir56D,*
219 were enriched in the *Gr5a*+ fraction compared to the input, while bitter receptor genes (*Gr66a* and
220 *Gr32a*) were depleted (Fig. S6B), indicating that the selection of *Gr5a*+ mRNAs was successful
221 and comparable to our prior experiments (Vaziri et al., 2020). However, compared to the marked
222 negative skew in gene expression we previously observed with a high sugar diet, where 90% of
223 genes had negative log2 fold changes, OSMI-differentially expressed genes (DEGs) showed a
224 similar distribution in positive and negative changes (Fig. S6C; Supplemental File 1)(Vaziri et al.,

225 2020). Indeed, further analyses revealed that OSMI treatment *reverted* (i.e., showed the opposite
226 direction of change; q<0.1, Wald test) or *restored* (practical equivalence test using a null
227 hypothesis of a change of at least 1.5-fold and q <0.05) the expression of 52% of the DEGs with
228 a SD/CD change (Fig. 3F, gray are downregulated and red are upregulated), and that most of the
229 genes changed with OSMI treatment (367) were also similarly affected by a loss of function
230 mutation in *Pcl* (Fig. 3F). Notable among these were the homeobox *cad* and *Ptx1 and* their
231 regulons, which have been implicated in taste function and plasticity (Fig. S6D) (Vaziri et al.,
232 2020). The genes affected y OSMi treatment were enriched in metabolic and neural processes,
233 such as chemical synapse transmission, synaptic target attraction, cell differentiation, and
234 detection of chemical stimuli (Fig. 3G and S7). These experiments place *OGT* and PRC2.1 in the
235 same genetic pathway that directs diet-induced taste plasticity at the chromatin, transcriptional,
236 and behavioral levels. They also argue that the activity of the metabolic sensory OGT may provide
237 the nutrient-dependent context for PRC2.1-mediated changes in chromatin accessibility.

238

239 **Sr is enriched at OGTx PRC2.1 genes and necessary for sweet taste function.**

240 Our data show that OGT orchestrates responses to the dietary environment in the sensory
241 neurons. Metabolic flux and the utilization of metabolite pools can be cell-specific, but most, if not
242 all, cells would experience higher OGT activity in response to the high sugar environment (Hart,
243 2019; Olivier-Van Stichelen et al., 2017). Cell-independent outcomes could arise from the
244 chromatin landscape and PRC2.1 occupancy unique to the Gr5a+ neurons. Still, these do not
245 necessarily provide a specific context to enact changes based on real-time nutritional data. A
246 parsimonious integration between nutrients and cellular context (i.e., neural activity) could occur
247 at the chromatin/transcriptional level. To investigate this possibility, we examined the regulatory
248 regions of OGT x Pcl and OGT x PREs (Polycomb Responsive Elements, DNA motifs to which
249 Polycomb Proteins bind) loci for enriched cis-regulatory motifs (Fig. S8A and B, Supplemental
250 File 1; note that a TF may appear multiple times as dots in this graph because of different binding
251 motifs). In this analysis, the highest log2 fold enrichments were for Polycomb Group proteins like
252 *PhoRC* (1.018, p=0.0099) and Trx-recruiter *Trithorax-like* (*Trl*, 1.972, p=0.0099 and 0.803,
253 p=0.0099; *Trx* is antagonistic to PRC2.1), as well as transcription factors, such as the Zn-finger
254 immediate early gene *Stripe* (*Sr*, homolog of human Early Growth Response 2, EGR2, alias
255 Krox20), the nutrient-sensitive factor *Sterol-Responsive-Element Binding Protein* (SREBP), and
256 the paired domain *pox-neuro* (*poxn*, known to be required for sensory neuron specification)

257 (Supplementary Table 1). To determine if they affected sweet taste, we measured the proboscis
258 extension in response to sucrose when these genes were overexpressed or knocked down in the
259 Gr5a+ neurons. The only factor that affected sweet taste responses across low and high sucrose
260 concentrations was *Sr*, which also showed higher mRNA abundance in the sensory neurons of
261 SD-flies (Fig. S8C).

262 *Sr* is a conserved transcription factor induced by neural activity via the MAPK/ERK
263 pathway (Beckmann and Wilce, 1997; Chen et al., 2016; Gonzales et al., 2020) and is essential
264 for sensory nerve development and plasticity (Duclot and Kabbaj, 2017; Murphy et al., 1989). This
265 signaling pathway is stimulated by mitogens, such as TGF-β/Activin signaling, which increase
266 with sugar levels, eating, and neural activity in flies and mammals (Lavoie et al., 2020; Liu and
267 Chen, 2022; Wilinski et al., 2019). Of note, OGT x Pcl co-occupied loci were enriched in
268 MAPK/ERK targets (Fig. 2E, blue). Enrichment for Sr cis-regulatory motifs was modest at OGT
269 *or* Pcl loci (l2fc=0.196 and 0.398, respectively; $p<0.001$ in both cases via an approximate
270 permutation test) but strong at genes bound by both these factors (OGT x Pcl =0.429 and OGT x
271 PREs=0.976, $p<0.001$, permutation test) (Fig. 4A; Supplemental File 1). When we compared the
272 distribution of Sr sites around the regulatory regions of OGT x PRC2.1 genes (either together or
273 separately), we found a marked bias around the transcriptional start site (TSS) (Fig. 4B, top). In
274 contrast, genes that OGT or PRC2.1 did not occupy, were depleted for Sr binding sites at the TSS
275 (Fig. 4B, bottom). This suggests that Sr predominantly occurs at genes that are bound by OGT
276 *and* PRC2.1. To this end, when we examined the expression of Sr-targets in the Gr5a+ neurons
277 of flies on the two diets, we noticed that these genes had negative log2 fold changes on the sugar
278 diet; this repression, however, was abolished by mutations in *Pcl* and by inhibition of OGT activity
279 (Fig. 4C, compare gray vs. pink and green, respectively). This hints toward functional cooperation
280 between *Sr* and *OGT/PRC2.1*. Importantly, since OGT and PRC2 are not always found at TSS,
281 the bias in *Sr* distribution at the TSS of "OGT/PRC2 regulated genes" indicates that coordination
282 between Sr and OGT/PRC2 may arise not from direct interactions but rather from two distinct
283 paths of information flow.

284 To characterize the effects of *Sr* on neural activity and behavior, we used the UAS/GAL4
285 system to overexpress this gene in the Gr5a+ neurons of adult flies. Overexpression of *Sr* resulted
286 in lower electrophysiological responses of the gustatory neurons to sucrose (Fig. 4D, Mann-
287 Whitney test, $p=0.001$) as well as lower PER at both high and low sucrose concentrations (Fig.
288 4E). This effect, however, was dependent on the catalytic activities of PRC2.1 and OGT. Indeed,
289 overexpression of *Sr* in flies treated with OSMI (green) or with an inhibitor of PRC2.1 (pink, EEDi,

290 used as in our previous work (Vaziri et al., 2020)) resulted in sucrose responses comparable to
291 those of control flies (Fig. 4F). Overall, these results argue for a role of *Sr* in taste plasticity in
292 coordination with *OGT* and *PRC2.1*.

293

294 **The ERK pathway modulates taste adaptations in response to diet.**

295 *Sr* is the downstream transcriptional effector for the Extracellular-signal Regulated Kinase
296 (ERK), a pathway stimulated by neural activity that plays a role in neuroplasticity (Lavoie et al.,
297 2020; Miningou and Blackwell, 2020; Thomas and Huganir, 2004) (Fig. 5A). We reasoned that
298 ERK/EGR2 might provide the sensory neurons with a specific context to drive cell-specific
299 outcomes under the same dietary environment. To test this hypothesis, we examined the role of
300 the kinase *rolled* (*rl*)– the ERK homolog in *D. melanogaster*– in sweet taste and diet-induced taste
301 plasticity.

302 First, we observed that, as with *Sr*, the mRNA abundance of *rolled* was higher in the Gr5a+
303 neurons of flies on a SD, but this gene was not a direct target of OGT or PRC2.1 (Fig. S9A). We
304 tried several available antibodies against *rolled* and activated (phosphorylated) *rolled* to establish
305 whether increased transcript levels also resulted in higher activation of this kinase; however, none
306 of them resulted in a reliable signal in our hands. We thus turned to genetic tools to investigate
307 whether higher rolled expression or activity played a role in sweet taste plasticity. To differentiate
308 between these two possibilities, we expressed either a wild-type *rolled* (rl^{WT}, Fig. 5B top, (Biggs
309 et al., 1994)) or constitutively active form of the kinase (rl^{Sem} Fig. 5B, bottom) (Oellers and Hafen,
310 1996) in the Gr5a+ neurons and tested neural and taste responses to sucrose. Overexpression
311 of rl^{WT} with *Gr5a-GAL4* did not affect the electrophysiological responses of the sensory neurons
312 to sucrose (Fig. 5C, *dark blue*); however, expression of the active rl^{Sem} decreased neuronal
313 responses to sucrose (Fig. 5C, *light blue*). These activity phenotypes were reflected in the
314 behavioral taste responses to sucrose, with rl^{WT} flies having identical PER to sucrose as controls
315 and rl^{Sem} showing reduced PER across high and low sucrose concentrations (Fig. 5D, *left vs.*
316 *right*; note that controls are shared here, plotted separately for clarity). Thus, *rolled* activity, but
317 not higher levels alone was sufficient to affect sweet taste plasticity. Not surprisingly, given the
318 known function of *rl/ERK* in neural activity, we found that this kinase was also necessary for sweet
319 taste responses, as loss of function mutants for *rolled* had lower electrophysiological and
320 behavioral responses to sucrose (Fig. S9B-C). To test whether there was a synergetic interaction
321 between *rl* and OGT, we repeated the same experiments in the presence of the OGT inhibitor

322 OSMI. Strikingly, OSMI treatment almost entirely blocked the effects of *rl*^{Sem} on both neural and
323 behavioral responses to sucrose (Fig. 5E-F).

324 To characterize the function of the *rl/Sr* pathway on taste plasticity, we used Trametinib,
325 a drug that inhibits ERK activation in animals (currently used for treating melanoma). At
326 concentrations previously used in flies (15.6mM) (Castillo-Quan et al., 2019; Slack et al., 2015),
327 Trametinib blocked the effects of *rl*^{Sem} expression on sweet taste responses (Fig. S10A).
328 Treatment with this ERK inhibitor also negated the effects of *Sr* overexpression on sucrose
329 responses, resulting in flies with PER comparable to controls (Fig. S10B). Thus, Trametinib
330 treatment efficiently blocks ERK signaling. To determine if the activity of the *rl/Sr* (ERK/Krox20)
331 pathway was necessary for taste plasticity in response to the sugar diet environment, we fed flies
332 a control or sugar diet with or without Trametinib for 7 days, then measured their neural and
333 behavioral responses to sucrose. Exposure to a high sugar diet decreases the
334 electrophysiological (Fig. 6A) and behavioral (Fig. 6B) responses to sucrose. However, when *rl*
335 activity was blocked with Trametinib, there was no decrease in neural responses or PER (Fig. 6C
336 and 6D). Of note, Trametinib had a minor but significant effect on sweet taste activity (compare
337 CD of Fig. 6C with CD of Fig. 6D), consistent with the observation that *rl* is necessary for normal
338 sweet taste function (Fig. S9B). Together, these data indicate that the ERK pathway plays a
339 critical role in the development of taste adaptations in response to diet and place its function
340 upstream of OGT.

341

342 **DISCUSSION**

343 Nutrigenomic signaling plays a function in health and disease by bridging the dietary
344 environment with physiological adaptations. However, the molecular mechanisms and
345 consequences of this type of nutrient sensing are still poorly understood. In particular, how
346 nutrigenomic signals are integrated with cellular contexts to drive specific outcomes has
347 remained hard to define due to the lack of mechanistic nutrigenomic models (Müller and
348 Kersten, 2003; Vaziri and Dus, 2021). In this work, we exploited the conserved phenomenon of
349 diet-induced taste plasticity and the genetic tools of the *D. melanogaster* fly to answer these
350 questions.

351 Here we report that the metabolic enzyme OGT is associated with neural chromatin at
352 introns and transcriptional start sites. While OGT-associated genes showed subtle but

353 significant changes in chromatin accessibility in response to diet, these dynamics were much
354 more robust at loci co-occupied by both OGT and the epigenetic silencer PRC2.1. At genes
355 decorated by both factors, we observed sizable diet-dependent chromatin variations that were
356 critically dependent on the catalytic activity of OGT. OGT activity was also necessary for the
357 differential transcriptional and taste responses to the high-sugar diet. The OGT and PRC2
358 bound nutrient-dependent loci were enriched for binding motifs for the activity-dependent
359 transcription factor Sr, the effector of the ERK pathway. We show that this signaling pathway
360 functions upstream of OGT/PRC2.1 to shape neural and behavioral taste responses to the
361 dietary environment. We thus propose a model where a nutrigenomic pathway composed of
362 OGT and PRC2 integrates information from the nutrient and cellular environment via ERK
363 signaling to orchestrate specific responses to diet (Fig. 6E). This integration occurs at the level
364 of chromatin and modulates the expression of transcription factors and signaling regulators that
365 further amplify and extend the reach of nutrigenomic signaling. Our findings reveal how
366 nutrigenomics contributes to crucial neural plasticity and behavior aspects.
367

368 **OGT and Chromatin Dynamics.**

369 OGT is a conserved enzyme that catalyzes the transfer of UDP-GlcNAc to the serine
370 and threonine residues of proteins (Hart, 2019; Olivier-Van Stichelen et al., 2017). Because
371 UDP-GlcNAc synthesis by the Hexosamine Biosynthesis Pathway (HBP) combines sugar,
372 amino acid, nucleotide, and fatty acid metabolism, the levels of this metabolite, as well as the
373 activity of the enzymes in this pathway, are inextricably linked to cellular metabolism and diet
374 (Hart, 2019; Olivier-Van Stichelen et al., 2017). Higher HBP flux directly impacts OGT activity
375 because the function of this enzyme is linear across a vast range of physiological UDP-GlcNAc
376 concentrations. Because of this, OGT is recognized as a critical nutrient sensor in animal
377 physiology, particularly in development, cancer, and metabolic disease (Hart, 2019; Olivier-Van
378 Stichelen et al., 2017). More recently, its importance for neural function and plasticity has also
379 been recognized, with studies implicating it in synapse maturation, neural excitability, activity,
380 and plasticity (Ardiel et al., 2018; Butler et al., 2019; Giles et al., 2019; Hwang and Rhim, 2019;
381 Lagerlöf et al., 2017, 2016; Li et al., 2019; May et al., 2019; Ruan et al., 2014; Su and Schwarz,
382 2017). Our group showed that a high sugar diet acutely and chronically increased HPB activity
383 in flies and played a role in diet-induced sensory plasticity (May et al., 2019; Wilinski et al.,
384 2019).

385 OGT is a nucleocytoplasmic enzyme, and the GlcNAc modification is enriched in nuclear
386 and synaptic proteins, which extends its reach on cellular physiology (Hart, 2019; Olivier-Van
387 Stichelen et al., 2017). Although OGT is thought to play a role in gene regulation, only one study
388 has shown its direct association with chromatin in murine embryonic stem cells (Vella et al.,
389 2013). Here we show that OGT also decorates neural chromatin in *Drosophila melanogaster*.
390 Similar to embryonic stem cells, OGT was enriched at introns and transcriptional start sites and
391 primarily associated with transcriptionally active chromatin. However, we found that a portion of
392 OGT was also enriched at Polycomb repressive chromatin, consistent with previous reports that
393 the GlcNAc modification is found at PREs, as well as on many PcG proteins; OGT is also
394 associated with PcG complexes to mediate Hox-gene repression (Hart, 2019; Olivier-Van
395 Stichelen et al., 2017; Schuettengruber et al., 2017). On a high-sugar diet, there was a higher
396 association of OGT with DNA but lower chromatin accessibility. However, the magnitude of
397 these changes depended on what other regulatory and DNA-binding factors were found at OGT
398 loci. At loci with PRC2.1 binding and Sr/EGR2 motifs, chromatin openness was markedly
399 reduced in response to the high-sugar diet environment. To the best of our knowledge, this is
400 the first study to show that OGT-associated chromatin is nutrient-sensitive. Importantly, this
401 nutrient sensitivity was entirely dependent on the catalytic activity of OGT because it was
402 abolished in the presence of the inhibitor OSMI-1. Interestingly, OGT activity had no effect on
403 PRC2.1 association with co-occupied loci (and only a small effect at non-OGT loci, data not
404 shown). The H3K27 methylation activity of PRC2.1 is required for changes in chromatin
405 accessibility, including those that depend on diet in the sensory neurons (Schuettengruber et al.,
406 2017; Vaziri et al., 2020). Thus, our data suggest that OGT activity affects the repressive action
407 of PRC2.1.
408
409 These findings raise several important questions about the biochemical mechanisms of
410 OGT action that our genetic system is poorly suited to address, but that will be important to
411 define in future studies. First, what are the targets of OGT at nutrient-sensitive loci? Is OGT
412 directly GlcNAcylating PRC2.1 to modify its repressive drive? Several studies have linked OGT
413 activity with the stability, chromatin occupancy, or catalytic function of Polycomb Group Proteins
414 (Hart, 2019; Olivier-Van Stichelen et al., 2017). OGT influences stability and silencing activity of
415 the PRC2 subunit Enhancer of Zeste Homologue 2 (Ezh2) –the enzyme that catalyzes H3K27
416 methylation; knockdown of OGT decreased H3K27 methylation and Ezh2 occupancy at
417 promoters in cell culture, while OGT overexpression increased it (Chu et al., 2014; Sakabe and
418 Hart, 2010). OGT also affected the binding of Ezh2 to promoters of transcription factors in

419 breast cancer cells, but not its stability (Forma et al., 2018). Depending on cell type and tissue,
420 GlcNAcylation of Ezh2 did not affect its association with PRC2 but decreased its enzymatic
421 activity (Lo et al., 2018) or stability (Jiang et al., 2019; Sui et al., 2020; You et al., 2021). Further,
422 OGT-dependent recruitment of PRC2.1 to *UNC5* family gene promoters led to their silencing in
423 HCT116 colon cancer cells, which has been linked to the worsening of colorectal cancer by a
424 high carbohydrate diet in mammals (Decourcelle et al., 2020). In the hippocampus, knockdown
425 of *OGT* reduced PRC2.1-mediated gene silencing during fear memory consolidation (Butler et
426 al., 2019); GlcNAcylation of Polyhomeotic– motifs which are enriched at OGT x Pcl sites in our
427 data– was also required for its repressive properties (Gambetta et al., 2009; Gambetta and
428 Müller, 2014). Thus, converging evidence suggests that OGT impacts different aspects of PRC2
429 and PcG biology and is broadly consistent with our data. Connections between OGT and ERK
430 have also been uncovered in the context of cancer and cell division, with studies showing that
431 inhibition of ERK signaling decreases O-GlcNAcylation and vice-versa (Jiang et al., 2016;
432 Zhang et al., 2015) and that GlcNAcylation promotes ERK-effects while OGT inhibition blocks
433 them (Cork et al., 2018; Lei et al., 2020; Weiss et al., 2021). These findings are consistent with
434 the effect and direction of the genetic interactions we observed between OGT and PRC2.1 and
435 OGT and ERK, the direction of "information flow" within the cell (Fig. 6E), and the effects of our
436 genetic manipulations. OGT could also affect chromatin accessibility by GlcNAcylating histones,
437 although the function and effects of these histone modifications are still poorly understood
438 (Gambetta and Müller, 2015; Hirosawa et al., 2018; Konzman et al., 2020; Olivier-Van Stichelen
439 et al., 2017). Another outstanding question is how OGT is targeted to chromatin and whether
440 this recruitment is dynamic and related to nutrient availability. For example, are there different
441 local pools of OGT and GlcNAc in the nucleus vs. cytoplasm (or mitochondria) where OGT has
442 been described? Finding answers related to cellular compartmentalization of this metabolic
443 enzyme and its targets will be an essential step in understanding nutrient signaling, currently
444 one of the central questions in the field.
445
446 **Sensors and effector mechanisms of nutrigenomic signaling.**
447 OGT provides an instructional role in cellular adaptations to the dietary environment, as
448 our data and that of others suggest (Hart, 2019; Olivier-Van Stichelen et al., 2017). But OGT is
449 active in every cell, so what determines the specificity of outcomes? The first mode of specificity
450 is likely permissive and related to the general accessibility of genomic loci to change: those
451 silenced during development would also be shielded from the effects of environmental variation.

452 However, prescriptive mechanisms should also exist. In the case of the sweet taste
453 neurons, sugar directly activates the cells via receptor-dependent mechanisms and enhances
454 OGT's metabolic activity. Integration of these two signals– a synergy almost entirely unique to
455 these cells– could shape cell-specific outcomes. Our data support this idea by revealing a
456 function for the mitogen-activated protein kinase ERK in neural and behavioral taste
457 adaptations. *rl/ERK* and its effector, *Sr/EGR2* mRNAs, were higher in the Gr5a+ neurons of flies
458 on a sugar diet. Binding sites for the ERK effector Sr/EGR2 are among the most enriched at
459 OGT x Pcl/PRE loci, and several of these co-occupied genes are known to be regulated by
460 ERK, like the transcription factor c-fos (*kayak*).
461 Further evidence of ERK/EGR2 interactions with OGT/PRC2 comes from the observations that
462 diet-driven changes in Sr/EGR2 regulons, as well as the effects of Sr overexpression on sweet
463 taste, depended on the activity or presence of OGT and PRC2. Most importantly, we
464 demonstrate that this pathway affects taste plasticity at both the neurophysiological and
465 behavioral levels, with strong epistatic interactions with OGT. Together, these molecular and
466 functional data support the idea that the activity-dependent ERK pathway provides the context
467 (likely neural activity) for cell-specific outcomes in response to the same nutrient environment. It
468 is worth noting that this pathway has the potential to tune plasticity to other nutrient-activity
469 fluctuations, such as those experienced with fasting and satiety, since flux through the HBP and
470 known-ERK activators, such as TGF-β, change with acute and chronic energy changes (Hart,
471 2019; Lavoie et al., 2020; Liu and Chen, 2022; Olivier-Van Stichelen et al., 2017; Papa et al.,
472 2019; Wilinski et al., 2019).
473
474 Finally, sensing mechanisms must be transformed into actions to be effective. This is
475 likely the role of PRC2.1. Only a small portion of the genes occupied by PRC2.1 is sensitive to
476 diet and OGT activity. PRC2.1 decorates chromatin at these sites already in the control diet
477 condition but redistributes (up or down) in response to the high sugar diet (Vaziri et al., 2020).
478 Thus, PRC2.1 is not binding to new loci but instead tuning the output of those it is already
479 bound to.
480 Further, OGT activity did not affect PRC2.1 occupancy at OGT x Pcl sites, suggesting that other
481 mechanisms mediate this effect. To this end, the Tudor domain of the mammalian orthologues
482 of Pcl, MTF2, binds H3K36m to promote the intrusion of PRC2.1 into active genes and drive
483 repression (Ballaré et al., 2012; Brien et al., 2012; Cai et al., 2013). This could be a potential
484 mechanism through which PRC2.1 is redistributed to transcribed loci in the sugar diet
485 environment. Perhaps activity- or nutrient-transcription could play a role in this process. What

486 mechanisms promote PRC2.1 activity or nutrient-dependent redistribution will be important to
487 define in the future but will be better addressed in vitro models.

488

489 **From nutrigenomics to neural plasticity**

490 In our model, metabolic and activity sensors integrate cellular information to promote
491 changes in gene expression. How are these actualized into physiological (in this case, neural)
492 adaptations that underlie behavior or disease? This is one of the central and unresolved
493 questions in nutrigenomics. Our model's genetic and neural tractability provides a unique
494 opportunity to get some answers. The 162 co-occupied loci identified were enriched for
495 transcription and regulatory factors involved in cell proliferation, differentiation, signaling, and
496 neural activity, as well as pathways implicated in neural plasticity. Many of these DNA binding
497 factors play essential roles during the development of sensory neurons to set their biophysical
498 properties, such as *Ptx1* and *cad*, but also affect adult taste plasticity. The regulons of these
499 TFs include genes known to affect pre and postsynaptic branching and structure, as well as
500 synaptic physiology. Thus our collective data indicate that this nutrigenomic pathway promotes
501 taste adaptations most likely by re-engaging developmental gene batteries, a mechanism that
502 has been hypothesized to play a role in neural plasticity (Hobert, 2011; Marder and Prinz, 2002;
503 Parrish et al., 2014; Vaziri et al., 2020). Whether this is a general rule of nutrigenomic signaling
504 or something specific to these sensory neurons is yet to be determined; however, it is
505 interesting to note that this is similar to how cancer cells exploit developmental networks for
506 uncontrolled growth (DeBerardinis and Chandel, 2016; Faubert et al., 2020).
507
508

509 **LIMITATIONS**

510 Although using sensory plasticity and fly gustatory neurons as a model to study
511 nutrigenomic signaling brings unique advantages, it also has significant limitations. These
512 primarily arise from the small number of cells (60) and the *in vivo* nature of our model. First, we
513 cannot probe whether OGT, PRC2, and EGR2 physically interact or modify each other in these
514 cells. Thus, evidence for our model arises from the combination of cell-specific molecular,
515 genetic, and physiological data. Second, we only inferred that the loci with Sr/EGR2 motifs
516 integrate activity due to the well-established function of the ERK pathway in activity-dependent

517 plasticity; future studies should address this directly and compare the effects of acute vs.
518 chronic nutrient influx.
519 Further, while inhibitors have allowed us to establish critical epistatic interactions and
520 conduct dietary manipulations while bypassing developmental effects and genetic challenges,
521 we cannot exclude that some of these effects may be non-cell autonomous. Integrating this
522 model with biochemical approaches that preserve the appropriate activity and nutrient context
523 would help address these critical questions. Finally, pathways beyond OGT, ERK, and PRC2.1
524 may also play a role in sensory plasticity.
525
526
527 **CONCLUSIONS**
528 In summary, we show that activity and nutrient sensing mechanisms are integrated at
529 the genomic level to promote neural adaptations to the food environment. In particular, our data
530 reveals a central and instructional role for OGT and meaningful epistatic interactions with
531 sensors (ERK) and effectors (PRC2.1). More generally, we put forth a model where cell and
532 context specificity transforms “nutritional data” – i.e., variations in nutrient and metabolite levels–
533 into nutritional information (Floridi, 2005), as shown in Fig. 6E (pink boxes). This information is
534 processed and interpreted by gene regulatory processes to make “decisions" about responding
535 to environmental challenges and carrying out physiological, neural, and behavioral changes.
536 Thus, nutrigenomic mechanisms could provide a critical path for information flow in biological
537 systems (Fabris, 2009; Reinagel, 2000; Shannon, 1948; Smith, 2000). A clear advantage could
538 reside in their ability to amplify transient, and often minor, variations in nutrient and activity
539 levels into strong reactions, which can be used to orchestrate responses to current *and* future
540 environmental challenges. Future studies in this field will no doubt uncover fascinating insights
541 about the rules of nutrigenomic communication: these discoveries will illuminate how nutrition
542 and gene expression converge to shape cell physiology and provide us with new tools to
543 promote wellness and diminish the burden of disease.
544

545 **METHODS**

546 **Fly husbandry, strains, and diets**

547 All flies were grown and fed cornmeal food (Bloomington Food B recipe) at 25°C and 45 to 55%
548 humidity under a 12-hour light/12-hour dark cycle (Zeitgeber time 0 at 9:00 AM.) unless otherwise
549 stated. Male flies were collected under CO_2 anesthesia 1-3 days after eclosion and maintained in
550 a vial that housed 35-40 flies. Flies were acclimated to their new vial environment for an additional
551 2 days and were moved to fresh food vials every other day. The GAL4/UAS system was used to
552 express transgenes of interest using the *Gustatory receptor 5a Gr5a-GAL4* transgene. For each
553 GAL4/UAS cross, transgenic controls were made by crossing the $w1118^{CS}$ (gift from A. Simon,
554 *CS* and *w1118* lines from the Benzer laboratory) to GAL4 or UAS flies, sex-matched to those
555 used in the GAL4/UAS cross. The fly lines used for this paper are listed in supplemental file 1.

556 For all dietary manipulations, the following compounds were mixed into standard cornmeal food
557 (Bloomington Food B recipe) (0.58 calories/g) by melting, mixing, and pouring new vials as in
558 (Musselman and Kühnlein, 2018) and (Na et al., 2013). For the 30% sugar diet (1.41 calories/g),
559 Domino granulated sugar (w/v) was added. Inhibitors were solubilized in 10% DMSO and added
560 to the control o sugar diet at a total concentration of 10 μM for OSMI (May et al., 2020; Ortiz-
561 Meoz et al., 2015), 8 μM for EEDi (Vaziri et al., 2020), and 15.6mM for Trametinib (Castillo-Quan
562 et al., 2019; Slack et al., 2015). Animals were assigned randomly to dietary groups. The sample
563 sizes were determined based on standards in the field. No animal was excluded from any of the
564 analyses.

565 **Proboscis extension response**

566 Male flies were food-deprived for 18 to 20 hours in a vial with a Kimwipe dampened with Milli-Q
567 filtered deionized water. Proboscis Extension Response was carried out as described in (Shiraiwa
568 and Carlson, 2007). Scoring of extension responses was conducted manually, and whenever
569 possible, experimenters were blinded. Experiments were replicated 2-3 times by two different
570 experimenters.

571

572 **Affinity purification of ribosome-associated mRNA (TRAP)**

573 Male fly heads (300 per replicate, ~10,000 *Gr5a+* cells) were collected using sieves chilled in
574 liquid nitrogen and dry ice. Frozen tissue was then lysed as previously described (Chen and

575 Dickman, 2017; Vaziri et al., 2020). From 10% of the total lysate, total RNA was extracted by
576 TRIzol LS Reagent (Thermo Fisher Scientific, 10296010) for input. The remainder of the lysate
577 was precleared by incubation with Dynabeads Protein G (Thermo Fisher Scientific, 10004D) for
578 2 hours and subsequently incubated with Dynabeads Protein G and an anti-Flag antibody (Sigma-
579 Aldrich, F1804) at 4°C with rotation for 2 hours, then RNA was extracted from ribosomes bound
580 to beads by TRIzol Reagent (Chen and Dickman, 2017).

581

582 **Targeted DNA adenine methyltransferase identification (TaDa) and Chromatin**
583 **Accessibility TaDa (CATada)**

584 To generate the *UAS-LT3-Dam::OGT* construct, the coding region of the *OGT* gene was amplified
585 from *w1118*^{CS} animals with the primers listed below and assembled into the *UAS-LT3-DAM*
586 plasmid (gift from A. Brand, University of Cambridge) using the NEBuilder HiFi DNA Assembly kit
587 based on the manufacturer's instructions (New England Biolabs). Transgenic animals were
588 validated by reverse transcription PCR targeting the correct insert. The *UAS-LT3-Dam::OGT* and
589 *UAS-LT3-Dam* line were crossed to the *Gr5a-GAL4*; *tubulin-GAL80*^{ts}. All animals were raised
590 and maintained at 20°C. Expression of *Dam::OGT* and *Dam* was induced at 28°C for 18 hours.
591 For all experiments, 300 heads of male and female flies were collected per replicate on dry ice by
592 sieving. DNA was extracted following kit instructions (Invitrogen). To identify methylated regions,
593 purified DNA was digested by Dpn I, followed by PCR purification of digested sequences. TaDa
594 adaptors were ligated by T4 DNA ligase (NEB). Adapter ligated DNA was PCR-amplified and
595 purified according to the protocol (Marshall et al., 2016). Purified DNA was digested with Dpn II,
596 followed by sonication to yield fragments averaging 300 base pairs. TaDa adaptors were removed
597 from sonicated DNA by digestion followed by PCR purification, and purified sonicated DNA was
598 used for library preparation (Vaziri et al., 2020) and (Marshall et al., 2016).

599 pUAST-Sxc.Forward gatctgGCCGGCGCaATGCATGTTGAACAAACACGAATAAATATG

600 pUAST-Sxc.Reverse gttccttcacaaagatcctTTATACTGCTGAAATGTGGTCCGGAAG

601

602 **Library preparation**

603 Generation of RNA sequencing (RNA-seq) libraries was with the Ovation SoLo RNA-seq System
604 for *Drosophila* (NUGEN, 0502-96). All reactions included integrated Heat-Labile Double-Strand

605 Specific DNase treatment (ArcticZymes, catalog no. 70800-201). The DNA-sequencing libraries
606 for TaDa were generated using the Takara ThruPLEX Kit (catalog no. 022818). For rat RNA-seq,
607 libraries were prepared using the Nugen Ovation Model organism (Rat #0349-32) with 1/10th
608 ERCC spike-in mix. These libraries were run on a NextSeq instrument using a HO 150 cycle cit
609 (75x75 bp paired-end reads). All *Drosophila* libraries were sequenced on the Illumina NextSeq
610 platform (High-output kit v2 75 cycles) at the University of Michigan Genomics Core facility.

611

612 **High-throughput RNA-seq analysis**

613 Fastq files were assessed for quality using FastQC (Andrews and Others, 2010). Reads with a
614 quality score below 30 were discarded. Sequencing reads were aligned by STAR (Dobin et al.,
615 2013) to dmel-all-chromosomes of the dm6 genome downloaded from Ensembl genomes.
616 Counting was conducted by HTSeq (Anders et al., 2015). Gene counts were used to call
617 differential RNA abundance by DESeq2 (Love et al., 2014). A pipeline was generated from
618 (Wilinski et al., 2019). To determine the efficiency and cell specificity of the TRAP, pairwise
619 comparisons were made between the *Gr5a*+-specific fraction and the input. For comparisons
620 between dietary conditions, DESeq2 was only applied to the *Gr5a*+-specific IP condition. SD7
621 and Pcl^{c429} datasets were analyzed from and described in (Vaziri et al., 2020). A cutoff of $q < 0.1$
622 was used to call DEGs. To identify overlap between datasets GeneOverlap was used (Shen and
623 Sinai, 2013).

624

625 **High-throughput TaDa and CATaDa analysis**

626 Fastq files were assessed for quality using FastQC (Andrews and Others, 2010). Reads with a
627 quality score below 30 were discarded. The damidseq_pipeline was used to align, extend, and
628 generate log2 ratio files (*Dam::Sxc/Dam*) in GATC resolution as described previously (Marshall
629 and Brand, 2015) and as in (Vaziri et al., 2020). Reads were mapped by Bowtie2 (Langmead and
630 Salzberg, 2012) to dmel-all-chromosomes of the dm6 genome downloaded from Ensembl
631 genomes, followed by read extension to 300 bp (or to the closest GATC, whichever is first). Bam
632 output is used to generate the ratio file in bedgraph format. Bedgraph files were converted to
633 bigwig and visualized in the UCSC Genome Browser. Principal components analysis plots
634 between biological replicates were computed by multibigwigSummary and plotCorrelation in
635 deepTools (Ramírez et al., 2016). Peaks were identified from ratio files using find_peaks (FDR

636 <0.01) (Marshall and Brand, 2015) and as in (Vaziri et al., 2020). Overlapping intervals or nearby
637 intervals (up to 50bp) were merged into a single interval using mergeBed in BEDtools (Quinlan
638 and Hall, 2010). Intervals common in at least 2 replicate peak files were identified by Multiple
639 Intersect in BEDtools and used to generate the consensus peaks (Quinlan and Hall, 2010). For
640 CATaDa experiments, all analyses were performed similarly to those of TaDa with the exception
641 that *Dam* only profiles were not normalized as ratios but shown as normalized binding profiles
642 generated by converting bam files to bigwig files normalized to 1× dm6 genome as reads per
643 genome coverage (Sequencing depth is defined as the total number of mapped reads times the
644 fragment length divided by the effective genome size). Binding intensity metaplots were made by
645 computing a matrix for specified regions (Ramírez et al., 2016). To determine the proportion of
646 genes that fit within the various chromatin domain subtypes, we first matched *Dam::OGT/Dam*
647 targets to coordinates identified by (Filion et al., 2010) and then determined their gene count in
648 each chromatin subtype (observed) compared to the whole genome (expected). Peak annotations
649 were conducted using the HOMER annotatePeaks tool (Heinz et al., 2010) with the dm6 reference
650 genome. In TaDa analysis, genes were considered targets of the factor being investigated if a
651 peak existed anywhere on their length.

652

653 **Pathway enrichment analysis**

654 For all fly experiments, GO term enrichment analysis was performed using the iPAGE package
655 (Goodarzi et al., 2009), using gene-GO term associations extracted from the Flybase dmel 6.08
656 2015_05 release. For all analyses, iPAGE was run in discrete mode. Independence filtering was
657 deactivated for all discrete calculations. All other iPAGE settings default values. All shown GO
658 terms pass the significance tests for overall information described in (Goodarzi et al., 2009). For
659 each term, bins that are outlined show especially strong contributions [*P* values such that a
660 Benjamini-Hochberg FDR (Benjamini and Hochberg, 1995) calculated across that row yields $q <$
661 0.05].

662

663 **Analysis of cis-regulatory enrichments**

664 For each *D. melanogaster* DNA binding protein motif available from the CIS-BP database
665 (Weirauch et al., 2014), we scanned the *D. melanogaster* genome (dmel 6.08 2015_05 release)
666 using the FIMO binding site discovery tool [cite :doi:10.1093/bioinformatics/btr614]. Hits for each

667 motif were retained as potential binding sites and used to calculate overlaps with other features
668 (e.g., OGT of Pcl sites), as noted. Permutation tests to assess significance were performed
669 through repeated application of the bedtools shuffle [cite: doi.org/10.1093/bioinformatics/btq033]
670 command to obtain 100 resamplings (Supplementary Table 1) or 1,000 resamplings (Figure 4) of
671 the feature location of interest, requiring non-overlap of the randomly placed features. For the
672 analysis in Supplementary Table 1, we separately considered each potential motif for each
673 transcription factor extracted from the CIS-BP database (separate motifs for the same factor are
674 denoted by the gene name followed by a "_#" suffix, with # and integer). In the case of analysis
675 of Sr binding sites in Figure 4, we obtained a merged set of potential Sr binding sites by filtering
676 potential binding sites at a q value threshold of 0.1 (acting separately for each motif) and
677 combining all of the locations that were counted as a potential binding site for any of the Sr motifs
678 available from CIS-BP. Enrichments of overlaps with OGT, Pcl, and PRE sites were calculated
679 by comparing the actual observed count of overlapping features with the mean overlap observed
680 across 1,000 random samplings of the Sr motif locations (preserving the chromosome on which
681 each motif is located during shuffling). For comparison of Sr motif locations with TSSs, we first
682 identified the (strandedness-aware) start location of all "gene," "mobile_genetic_element," or
683 "pseudogene" features from the dmel6 Genbank annotations and then categorized all of these
684 locations as "OGT/PRC2" or "Not OGT/PRC2" based on whether or not the gene was associated
685 with an OGT, Pcl, or PRE location (see Supplementary Tables for gene lists for each feature
686 type). The density of Sr motif hits (as defined above) was then calculated as a function of position
687 relative to the TSS.

688

689 **Electrophysiology**

690 Extracellular recording on labellar sensilla was performed using the tip recording method
691 (Delventhal et al., 2014). 10–13-day-old flies were anesthetized by short ice exposure. To
692 immobilize the proboscis, the reference electrode containing the Beadle-Ephrussi Ringer solution
693 was inserted through the thorax into the labellum. The neuronal firing in L-type sensilla was
694 recorded with a recording electrode (10-20 μm diameter) containing 25 mM sucrose dissolved in
695 30 mM tricholine citrate as electrolyte. The recording electrode was connected to TastePROBE

696 (Syntech, The Netherlands), and electrical signals were obtained using the IDAC acquisition
697 controller (Syntech). The signals were amplified (10x), band-pass-filtered (100-3000 Hz), and
698 sampled at 12 kHz. Neuronal firing rates were analyzed by counting the number of spikes for a
699 500 ms period starting from 200 ms after contact using the Autospike 3.9 software. Experimenters
700 were blinded in the initial characterization of the phenotypes and experiments were independently
701 performed at least 3 times.

702

703 **Data analysis and statistics**

704 Statistical tests, sample size, and *p* or *q* values are listed in each figure legend. One or two-way
705 repeated measure ANOVA with posthoc tests were used for all PER experiments. All behavioral
706 data were tested for normality, and the appropriate statistical tests were applied if data were not
707 normally distributed. For the RNA-seq expression datasets, we coupled our standard differential
708 expression with a test for whether each gene could be flagged as "significantly not different" --
709 i.e., a gene for which we can confidently state that no substantial change in expression occurred
710 (rather than just a lack of evidence for change, as would be inferred from a large p-value on the
711 differential expression test). Defining a region of practical equivalence as a change of no more
712 than 1.5-fold in either direction, we tested the null hypothesis of a change larger than 1.5-fold
713 using the gene-wise estimates of the SE in log2fold change (reported by Deseq2) and the
714 assumption that the actual l2fcs are normally distributed. Rejection of the null hypothesis is
715 evidence that the gene's expression is not changed substantially between the conditions of
716 interest. Python code for the practical equivalence test can be found on GitHub as
717 calc_sig_unchanged.py. All data in the figures are shown as means ± SEM, **** $P < 0.0001$, ***
718 $P < 0.001$, ** $P < 0.01$, and *$P < 0.05$, unless otherwise indicated.

719

720 **Data and material availability statement**

721 All high-throughput data are available at the GEO repository: GSE188757 and GSE146245. LT3-
722 Dam::OGT flies are available upon request; all other fly lines are available in the BDSC database.
723

Contributions:

Experiments and data analysis: AV, HS, MD, DW, PF

Project design: MD, AV, HS

Data Interpretation: MD, AV, HS, DW, PF

Manuscript writing: MD

Manuscript editing: MD, AV, HS, DW, PF

Project supervision and funding: MD

Acknowledgments: We thank the University of Indiana at Bloomington, the VDRC, the FLYORF stock collections, and all the investigators who shared fly lines with us. Julia Kuhn designed some of the graphics for the manuscript. We are grateful to Dr. Morteza Khabiri for assistance in the calculation of potential TF binding sites. **Funding:** This work was funded by NIH R00 DK-97141 and NIH 1DP2DK-113750, the Klingenstein-Simons Fellowship in the Neurosciences, the Rita Allen Foundation, and NSF CAREER 1941822 (all to MD), the Rackham Predoctoral Fellowship (to AV), NIH T32 DA007268 (DW), NIH P30 DK089503 (MD and DW), and NIH R35GM128637 (to PLF).

Conflict of interest: The authors declare no conflict of interest.

743 **FIGURE & LEGENDS**

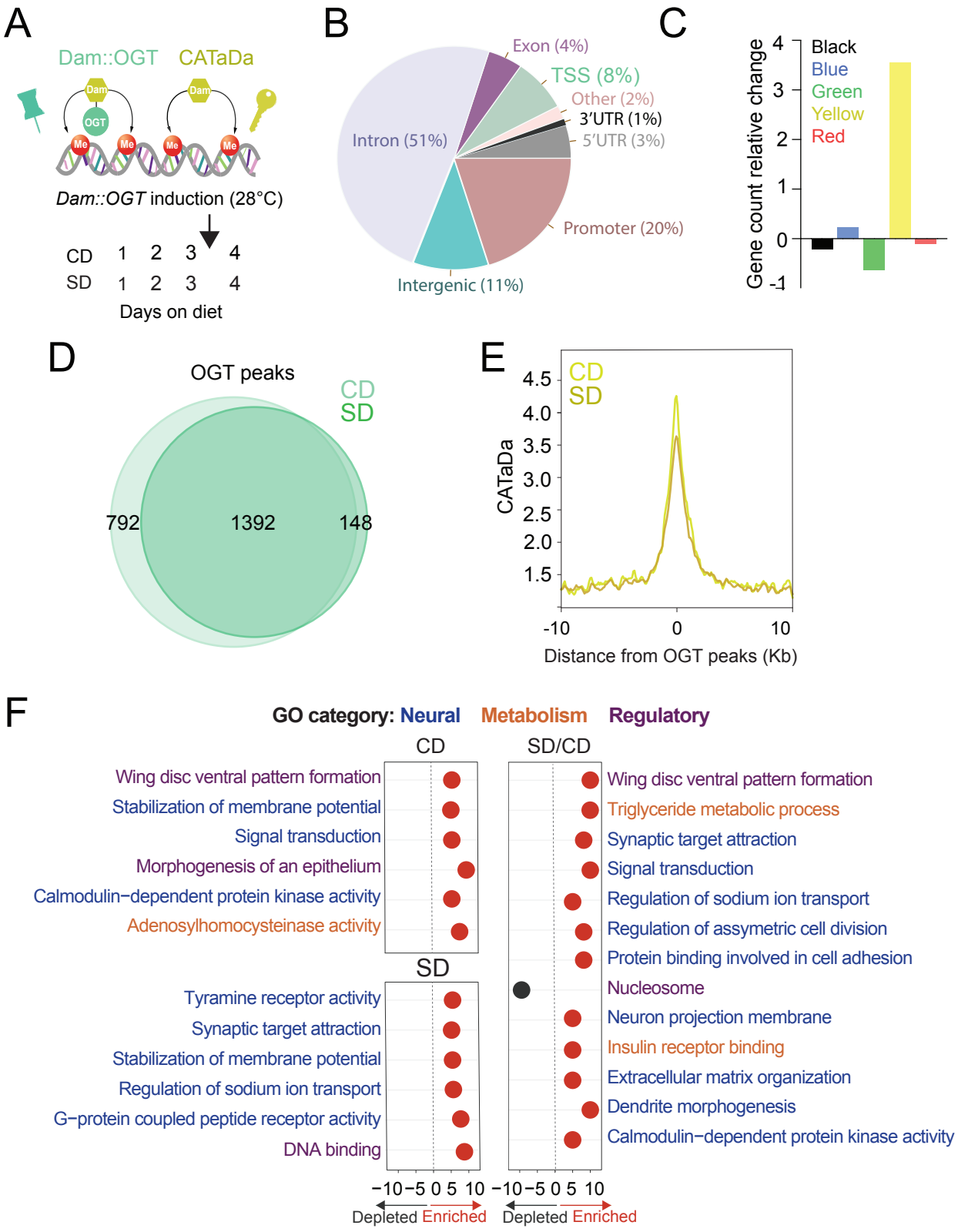
A
Dam::OGT
CATaDa
Dam
OGT
Me
Dam::OGT induction (28°C)
CD 1 2 3 4
SD 1 2 3 4
Days on diet
B
Exon (4%)
TSS (8%)
Other (2%)
3'UTR (1%)
5'UTR (3%)
Intron (51%)
Promoter (20%)
Intergenic (11%)
C
Gene count relative change
Black
Blue
Green
Yellow
Red
D
OGT peaks
CD
SD
792
1392
148
E
CD
SD
CATaDa
Distance from OGT peaks (Kb)
F
GO category: Neural Metabolism Regulatory
CD
SD/CD
Wing disc ventral pattern formation
Stabilization of membrane potential
Signal transduction
Morphogenesis of an epithelium
Calmodulin−dependent protein kinase activity
Adenosylhomocysteinase activity
SD
Tyramine receptor activity
Synaptic target attraction
Stabilization of membrane potential
Regulation of sodium ion transport
G−protein coupled peptide receptor activity
DNA binding
Wing disc ventral pattern formation
Triglyceride metabolic process
Synaptic target attraction
Signal transduction
Regulation of sodium ion transport
Regulation of assymetric cell division
Protein binding involved in cell adhesion
Nucleosome
Neuron projection membrane
Insulin receptor binding
Extracellular matrix organization
Dendrite morphogenesis
Calmodulin−dependent protein kinase activity
−10 −5 0 5 10
Depleted Enriched

744 **Figure 1: OGT decorates the chromatin of the sweet taste cells**

745 **(A)** Design of Targeted Dam-ID for OGT occupancy (*Dam::OGT*) and *Dam* accessibility (CATaDa)
746 experiments. Age-matched *Gr5a*;*tubulin-GAL80^{ts}* > *UAS-LT3-Dam::OGT* and *Gr5a*;*tubulin-*
747 *GAL80^{ts}>UAS-LT3-Dam* flies were placed on a CD or SD for 3 days at 20° to 21°C and then
748 switched to 28°C between days 3 and 4 to induce expression of the transgenes.

749 **(B)** Annotation of OGT chromatin occupied regions using HOMER.

750 **(C)** The proportion of observed *Dam::OGT* consensus peaks allocated to their respective
751 chromatin domains normalized to the expected proportions across the whole genome.

752 **(D)** Overlap of log2*(Dam::OGT/Dam)* chromatin binding peaks of CD (light green) and SD (dark
753 green) (find_peaks, q<0.01).

754 **(E)** Average CATaDa signal on a CD (light yellow) and SD (dark yellow) centered at OGT peaks.

755 **(F)** iPAGE summary plots for OGT peaks on a CD (top left), SD (bottom left), and the difference
756 of SD/CD (right). Text in blue represents neural GO terms, orange represents metabolic GO
757 terms, and purple represents regulatory GO terms.

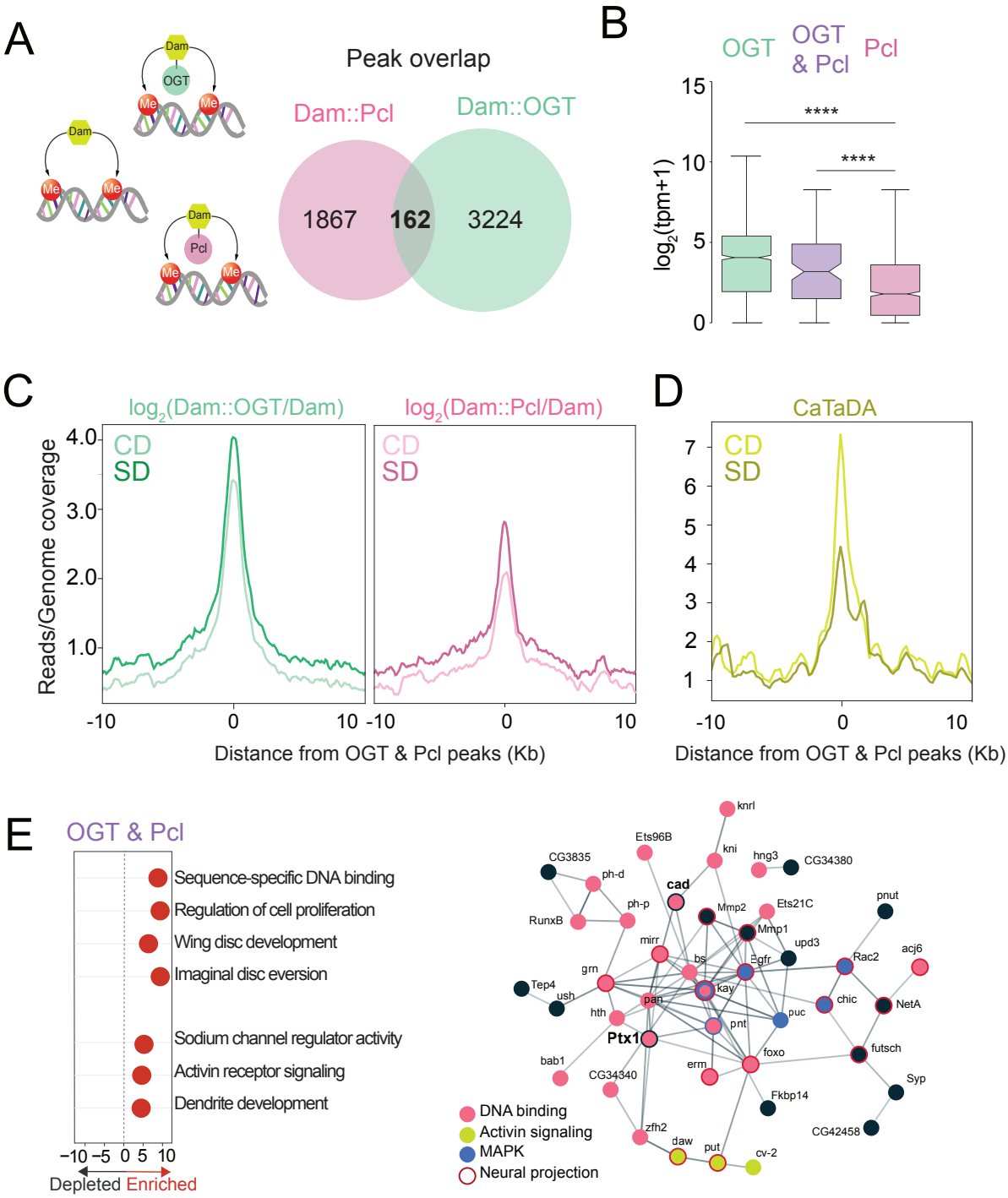
A
Dam
OGT
Me
Pcl
Peak overlap
Dam::Pcl
Dam::OGT
1867
162
3224
B
OGT
OGT & Pcl
Pcl
****
****
log2(tpm+1)
15
10
5
0
C
log2(Dam::OGT/Dam)
log2(Dam::Pcl/Dam)
CD
SD
Reads/Genome coverage
4.0
3.0
2.0
1.0
-10
0
10
Distance from OGT & Pcl peaks (Kb)
D
CaTaDA
7
6
5
4
3
2
1
E
OGT & Pcl
Sequence-specific DNA binding
Regulation of cell proliferation
Wing disc development
Imaginal disc eversion
Sodium channel regulator activity
Activin receptor signaling
Dendrite development
−10 −5 0 5 10
Depleted Enriched
knrl
Ets96B
kni
hng3
CG34380
CG3835
ph-d
cad
ph-p
RunxB
Mmp2
Ets21C
Mmp1
pnut
mirr
upd3
Rac2
acj6
bs
Egfr
grn
Tep4
ush
kay
pan
chic
NetA
hth
puc
pnt
Ptx1
foxo
futsch
bab1
erm
CG34340
Syp
Fkbp14
CG42458
zfh2
daw
put
cv-2
DNA binding
Activin signaling
MAPK
Neural projection

758 **Figure 2: OGT and PRC2.1 mark nutrient-sensitive chromatin in the sweet taste cells.**

759 **(A)** Diagram of the Targeted Dam-ID (TaDa occupancy, *Dam::OGT* green, and *Dam::Pcl* pink)
760 and (CATaDa, accessibility, yellow) experiments analyzed in this figure. Overlap of
761 log2(*Dam::Pcl/Dam*, pink) and log2(*Dam::OGT/Dam*, green) chromatin occupancy peaks (peak
762 calling: find_peaks, q<0.01).

763 **(B)** The distribution of the TPMs of genes occupied by OGT (green), Pcl (pink), and genes co-
764 occupied by OGT and Pcl (purple).

765 **(C)** Average log2(*Dam::OGT/Dam*; left) and log2(*Dam::Pcl/Dam*) (right) signal on a CD (lighter
766 shades) and SD (darker shades) diet centered at OGT + Pcl co-occupied peaks.

767 **(D)** Average CATaDa signal on a CD (lighter shade) and SD (darker shade) centered at OGT +
768 Pcl co-occupied peaks.

769 **(E) (left)** iPAGE pathway analysis of genes co-occupied by OGT and Pcl and **(**right**)** STRING
770 interaction network of genes co-occupied by OGT+Pcl, colors represent GO terms from the
771 pathway enrichment analysis.

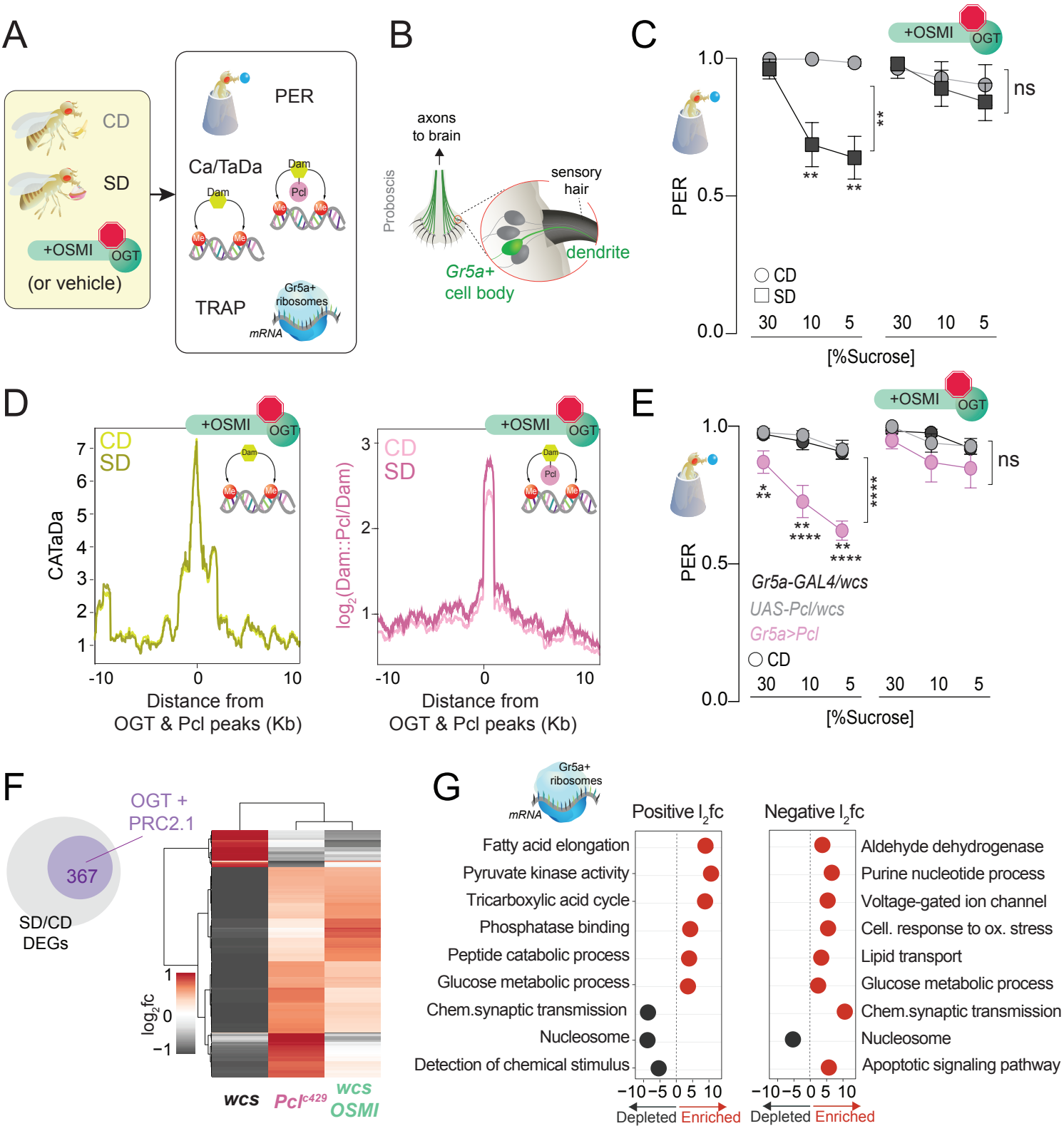
A
CD
SD
+OSMI
OGT
(or vehicle)
PER
Ca/TaDa
Dam
Pcl
Me
TRAP
Gr5a+ ribosomes
mRNA
B
axons to brain
Proboscis
sensory hair
dendrite
Gr5a+ cell body
C
+OSMI
OGT
PER
1.0
0.5
0.0
ns
**
CD
SD
30 10 5 30 10 5
[%Sucrose]
D
CD
SD
+OSMI
OGT
CATaDa
Distance from OGT & Pcl peaks (Kb)
log2(Dam::Pcl/Dam)
E
Gr5a-GAL4/wcs
UAS-Pcl/wcs
Gr5a>Pcl
****
F
OGT + PRC2.1
367
SD/CD DEGs
log2fc
wcs
Pcl c429
wcs OSMI
G
Gr5a+ ribosomes
mRNA
Positive l2fc
Negative l2fc
Fatty acid elongation
Pyruvate kinase activity
Tricarboxylic acid cycle
Phosphatase binding
Peptide catabolic process
Glucose metabolic process
Chem.synaptic transmission
Nucleosome
Detection of chemical stimulus
Aldehyde dehydrogenase
Purine nucleotide process
Voltage-gated ion channel
Cell. response to ox. stress
Lipid transport
Glucose metabolic process
Chem.synaptic transmission
Nucleosome
Apoptotic signaling pathway
−10 −5 0 5 10
Depleted Enriched

772 **Figure 3: OGT activity is necessary for chromatin, transcriptional, and behavioral**
773 **dynamics in response to the sugar diet environment.**

774 **(A)** Experimental design for the dietary epistasis experiments; control and experimental flies in C-
775 G were exposed to a control or sugar diet with vehicle (DMSO) or the OGT-inhibitor OSMI.

776 **(B)** Diagram of the anatomy of the sensory system showing the cell bodies, dendrites, and axons
777 of the sweet-sensing Gr5a+ neurons.

778 **(C)** Taste responses (*y-axis*) to stimulation of the labellum with 30, 10, and 5% sucrose (*x-axis*)
779 of age-matched male *w1118*^{cs} flies on a CD (circle) or SD (square) diet with vehicle (DMSO) or
780 10μM OSMI. n =14-17. Two way repeated measure ANOVA, main effect of OSMI treatment
781 *p=0.0089*; Tukey multiple comparisons test for 30, 10, and 5% sucrose: 1) CD vs. SD (DMSO)
782 p<0.05, *p=0.0090, p=0.0034* and 2) CD vs. SD (+OSMI), *p>0.05* at all concentrations.

783 **(D) (left)** Average CATaDa signal on a CD (light yellow) and SD (dark yellow) with OSMI-1
784 centered at *OGT+ Pcl* peaks (compare to Fig. 2D); **(right)** Average log2 Dam::Pcl/Dam signal on
785 a CD (light pink) and SD (dark pink) with OSMI-1 centered at *OGT+ Pcl* peaks (compare to Fig.
786 2).

787 **(E)** Taste responses (*y-axis*) to stimulation of the labellum with 30, 10, and 5% sucrose (*x* axis)
788 of age-matched male G*r5a>Pcl* (pink) and transgenic controls (shades of gray) on CD
789 supplemented with vehicle (DMSO, n=14-23) or 10 uM OSMI (n=20-42). Two Way Repeated
790 Measure ANOVA: 1) DMSO, main effect of genotype ****(*p<0.0001*) and genotype x
791 concentration (**p<0.05*); Tukey multiple comparisons test for 30, 10, and 5% sucrose
792 concentrations: *Gr5a>wcs vs. Gr5a>Pcl p=0.0165, p=0.0056, p=0.0025*; *Pcl>wcs vs. Gr5a>wcs,*
793 ns. 2) OSMI: main effect of genotype *p=0.3194* and genotype x concentration *p=0.6893*.

794 **(F)** Log_2fold (l2fc) of DEGs between SD/CD in *w1118cs* ± OSMI and Pcl^{c429} SD/CD.

795 **(G)** GO term analysis of the DEGs measured in the Gr5a+ neurons of flies fed a CD and SD
796 +OSMI.

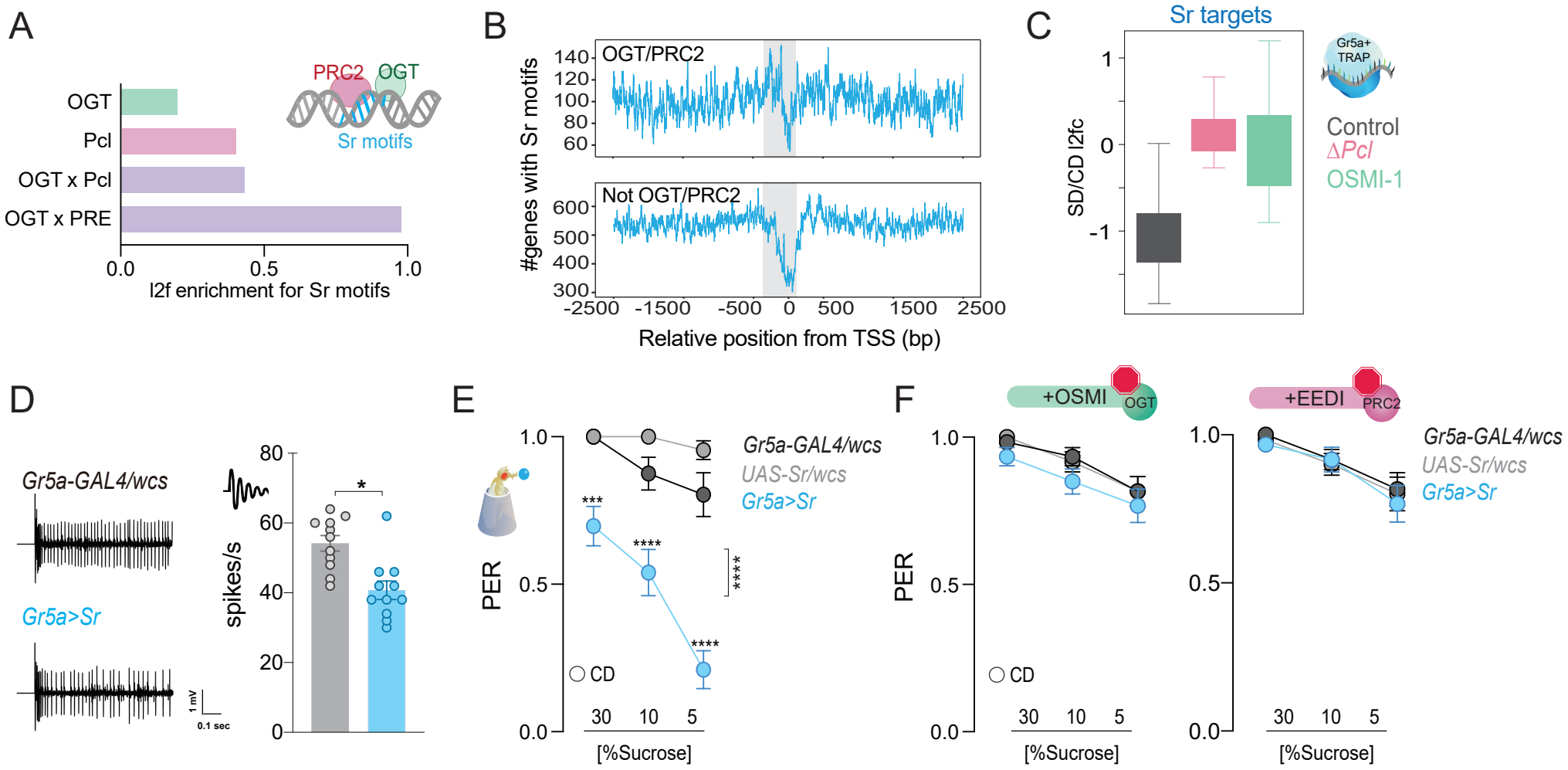
A
OGT
Pcl
OGT x Pcl
OGT x PRE
PRC2
OGT
Sr motifs
0.0
0.5
1.0
l2f enrichment for Sr motifs
B
OGT/PRC2
Not OGT/PRC2
#genes with Sr motifs
140
120
100
80
60
600
500
400
300
-2500
-1500
-500
0
500
1500
2500
Relative position from TSS (bp)
C
Sr targets
SD/CD l2fc
1
0
-1
Gr5a+ TRAP
Control
ΔPcl
OSMI-1
D
Gr5a-GAL4/wcs
Gr5a>Sr
1 mV
0.1 sec
spikes/s
80
60
40
20
0
*
E
PER
1.0
0.5
0.0
Gr5a-GAL4/wcs
UAS-Sr/wcs
Gr5a>Sr
***
****
****
****
CD
30
10
5
[%Sucrose]
F
+OSMI
OGT
+EEDI
PRC2
PER
1.0
0.5
0.0
CD
30
10
5
[%Sucrose]
Gr5a-GAL4/wcs
UAS-Sr/wcs
Gr5a>Sr

797 **Figure 4: The immediate early gene Sr is found at PRC2 x OGT genes and is involved in**
798 **sweet taste sensation.**

799 (A) Log_2fold (l2f) enrichment for Sr motifs at sites occupied by OGT (green), Pcl (pink), or
800 OGT+Pcl and OGT+PREs (purple), *p<0.0001*.
801 (B) Distribution of Sr motifs along the regulatory regions 2500 bp up and downstream the TSS
802 for the genes in (A).
803 (C) The distribution of RNA reads normalized as transcripts per million (TPMs) for genes that
804 have Sr sites and are expressed in the Gr5a+ neurons of flies on a CD and SD in control
805 flies or flies with mutations in *Pcl* or inhibition of OGT. *q>0.01*.

806 (D) Representative traces (left) and averaged neuronal responses to 25 mM sucrose
807 stimulation from the L-type sensilla of *Sr* overexpression flies (blue) and controls (gray).
808 n=11. Mann-Whitney test: *p*=0.001.
809 (E) Taste responses (*y-axis*) to stimulation of the labellum with 30, 10, and 5% sucrose (*x-*
810 *axis*) in *Sr* overexpression flies (blue) and controls (gray). n=22-38. Two way repeated
811 measure ANOVA, main effect of genotype *p<0.0001* and genotype x concentration
812 *p<0.0001*; Tukey post-test for multiple comparisons: 30%: ****p=0.0002* for *Gr5a>Sr*
813 compared to each control, 10%: *Gr5a>Sr vs. Gr5a>wcs p=0.0025* and *Gr5a>Sr vs.*
814 *Sr>wcs p<0.0001*; 5%: ****p*=0.0001 for *Gr5a>Sr* compared to each control. *Gr5a>wcs vs.*
815 *Sr>wcs p>0.05* at all concentrations.
816 (F) Taste responses (*y-axis*) to stimulation of the labellum with 30, 10, and 5% sucrose (*x-*
817 *axis*) in *Sr* overexpression flies (blue) and controls (gray) treated with the OGT inhibitor
818 OSMI (green) or the PRC2 inhibitor EEDi (pink). n=30. Two-way repeated measure
819 ANOVA, main effect of genotype *p=0.2993* and *p=0.9146* and genotype x concentration
820 *p=0.9293* and *p=0.9146,* respectively.

Sung Vaziri
Fig. 5

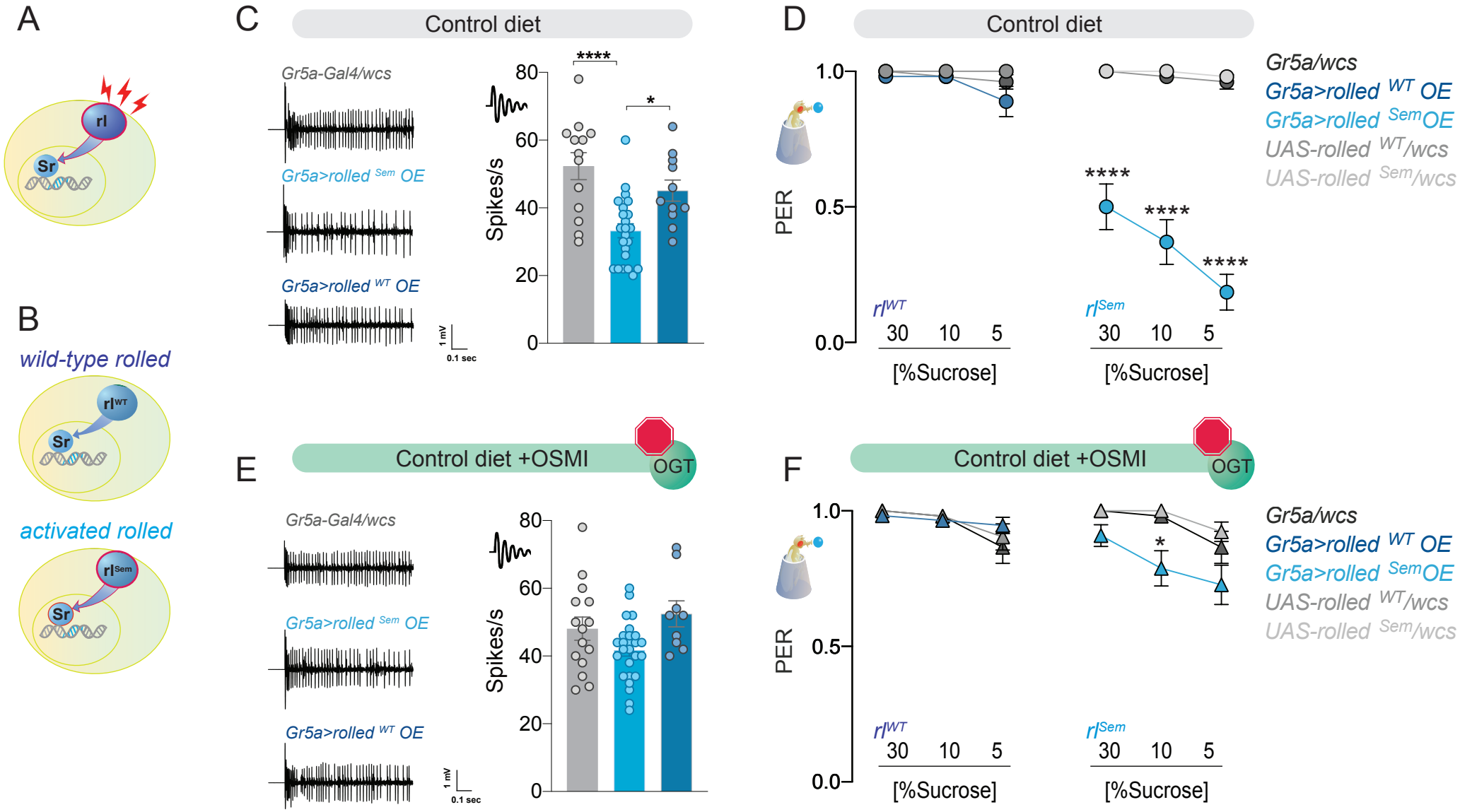

821 **Figure 5: The effect of the kinase rl/*ERK* on sweet taste depends on OGT activity.**

822 A. Diagram of the rl/ERK > Sr pathway, red sparks represent neural activity, and red outline
823 represents activation.
824 B. Diagram of the two types of rl/ERK transgenes used.
825 C. Representative traces (left) and averaged neuronal responses to 25 mM sucrose of L-type
826 sensilla in overexpression of wild-type (rl^{WT}) or constitutively active (rl^{Sem}) rl/ERK in the
827 Gr5a+ neurons (blue) and control (gray) on a CD. n=11-23. One way ANOVA; Tukey's
828 multiple comparison test: $p<0.0001$ for *Gr5a/+* vs. *Gr5a>*rl^{Sem}, $p=0.279$ for *Gr5a/+* vs.
829 *Gr5a>*rl^{WT}, and $p=0.018$ for *Gr5a>*rl^{Sem} vs. *Gr5a>*rl^{WT}.
830 D. Taste responses (*y-axis*) to stimulation of the labellum with 30, 10, and 5% sucrose (*x-*
831 *axis*) in flies with overexpression of wild-type (rl^{WT}) or constitutively active (rl^{Sem}) rl/ERK in
832 the Gr5a+ neurons (blue) and control (gray) flies on a CD+vehicle (DMSO). n=24-27. Two-
833 way repeated measure ANOVA, main effect of genotype $p<0.0001$ and concentration x
834 genotype $p<0.0001$. Tukey multiple comparisons tests: $p<0.0001$ for *Gr5a>*rl^{Sem} vs. all
835 other genotypes at 30, 10, and 5% and $p>0.05$ for all other comparisons at all
836 concentrations.
837 E. Representative traces (left) and averaged neuronal responses to 25 mM sucrose of L-type
838 sensilla in overexpression of wild-type (rl^{WT}) or constitutively active (rl^{Sem}) rl/ERK in the
839 Gr5a+ neurons (blue) and control (gray) on a CD+OSMI. n=11-23. One way ANOVA;
840 Tukey's multiple comparison test: $p=0.172$ for Gr5a/+ vs. *Gr5a>*rl^{Sem}, $p=0.603$ for Gr5a/+
841 vs. *Gr5a>*rl^{WT}, and $p=0.034$ for *Gr5a>*rl^{Sem} vs. *Gr5a>*rl^{WT}
842 F. Taste responses (*y-axis*) to stimulation of the labellum with 30, 10, and 5% sucrose (*x-*
843 *axis*) in flies with overexpression of wild-type (rl^{WT}) or constitutively active (rl^{Sem}) Rl/ERK
844 in the Gr5a+ neurons (blue) and control (gray) in flies fed a CD+OSMI. n 26=33. Two-way
845 repeated measure ANOVA, main effect of genotype $p=0.005$; Tukey multiple comparisons
846 tests: $p>0.05$ for all other comparisons at all concentrations except for $p<0.0001$ for
847 *Gr5a>*rl^{Sem} vs. rl^{Sem}*/wcs* at 10% $p=0.0216$. Effect of OSMI vs. vehicle: *Gr5a>*rl^{Sem} 30%
848 $p=0.0012$, 10% $p=0.0030$, 5% $p<0.0001$, and $p<0.05$ for all other genotypes.
849

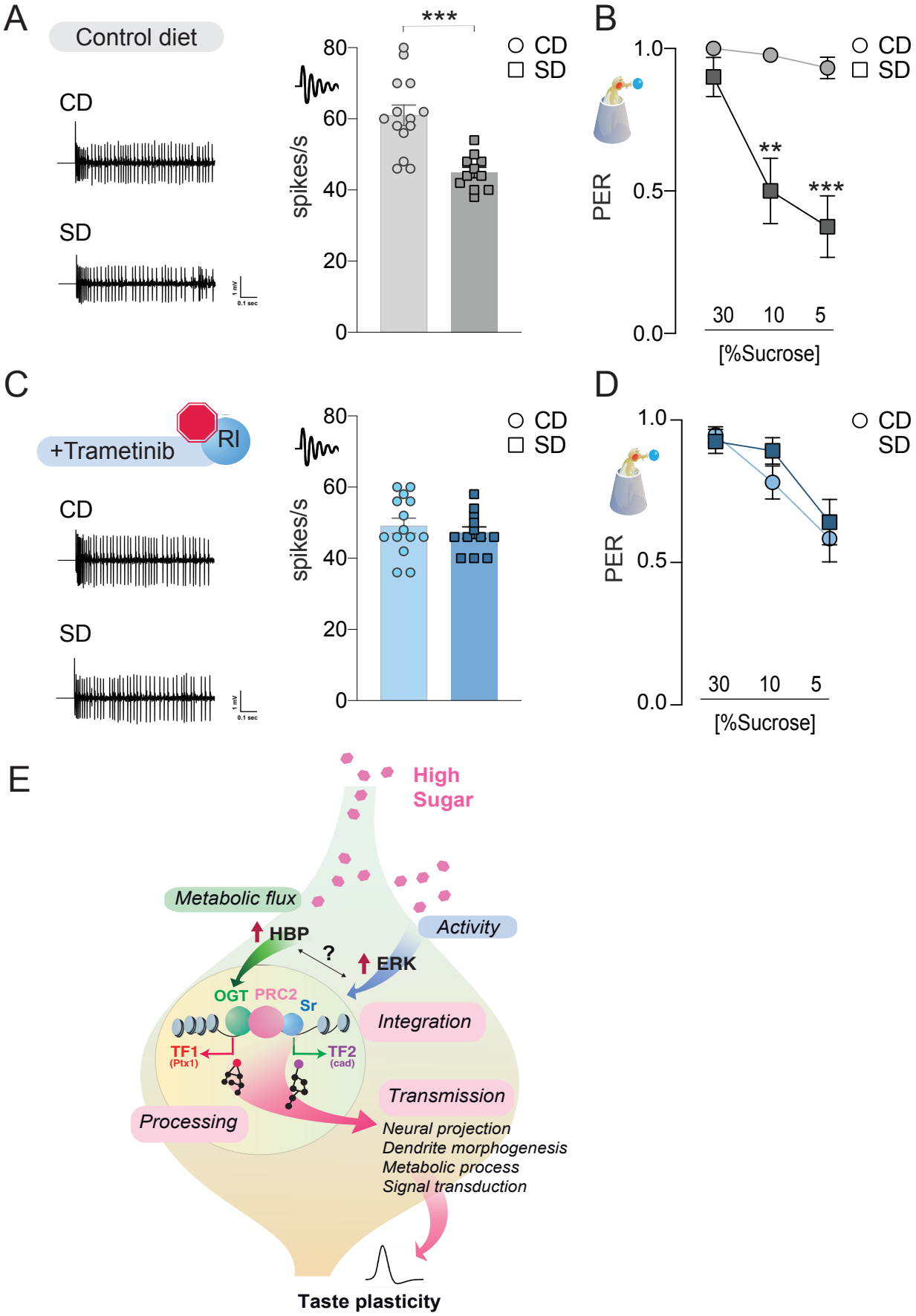
A
Control diet
CD
SD
spikes/s
80
60
40
20
0
***
CD
SD
B
PER
1.0
0.5
0.0
**
***
30
10
5
[%Sucrose]
C
+Trametinib
RI
D
E
High Sugar
Metabolic flux
Activity
HBP
?
ERK
OGT
PRC2
Sr
Integration
TF1
(Ptx1)
TF2
(cad)
Transmission
Processing
Neural projection
Dendrite morphogenesis
Metabolic process
Signal transduction
Taste plasticity

850 **Figure 6: The rl>Sr pathway is important for taste adaptations in response to diet.**

851 **A and C)** Representative traces (left) and averaged responses to 25 mM sucrose from L-type
852 sensilla of flies fed a CD and SD (**A**, gray) or Trametinib (**C**, blue). n=11-14. Unpaired t-test:
853 *p*=0.0001 for CD vs. SD, and *p*=0.486 for CD Trametinib vs. SD Trametinib.

854 **B and D)** Taste responses to stimulation of the proboscis with sucrose in flies fed a CD and SD
855 + vehicle (**B**, DMSO, gray) or Trametinib (**D**, blue). PER, n=20-33. PER: Two way repeated
856 measure ANOVA, main effect of diet, vehicle $p<0.0001$ and Trametinib $p=0.4701$; Tukey multiple
857 comparison test: vehicle CD vs SD 30% $p=0.421$, 10% $p=0.0017$, and 5% $p=0.0002$ and
858 Trametinib CD vs SD 30% $p=0.9702$, 10% p=0.4470, and 5% $p=0.9575$. Effect of Trametinib: CD
859 vehicle vs CD Trametinib, 30% $p=0.1745$, 10% $p=0.0108$, 5% $p=0.0015$; SD vehicle vs SD
860 Trametinib, 30% $p=0.4837$, 10% $p=0.0228$, 5% $p= 0.2339$.

861 **E)** A model for how OGT, PRC2, and ERK orchestrate taste plasticity in response to a changing
862 food environment. Boxes in pink describe the different steps of information processing (see
863 discussion).

SUPPLEMENTARY FIGURES & LEGENDS

Sung Vaziri
Supplement 1

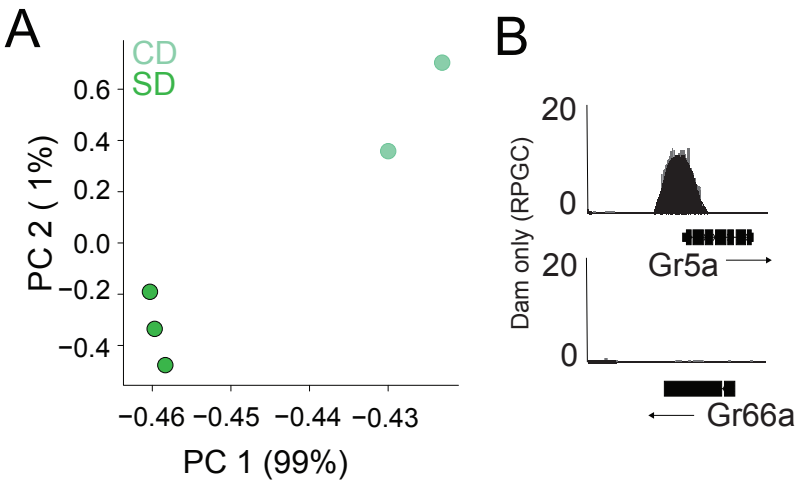

865 **Figure S1- Related to Figure 1, OGT resides on the chromatin of the *Gr5a*+ neurons**

866 **(A)** Principal component analysis of normalized log2(*OGT::Dam/Dam*) flies on CD (light green) or
867 SD (dark green).

868 **(B)** CATaDa from control diet flies at the sweet gustatory receptor *Gr5a* and the bitter gustatory
869 receptor *Gr66a*.

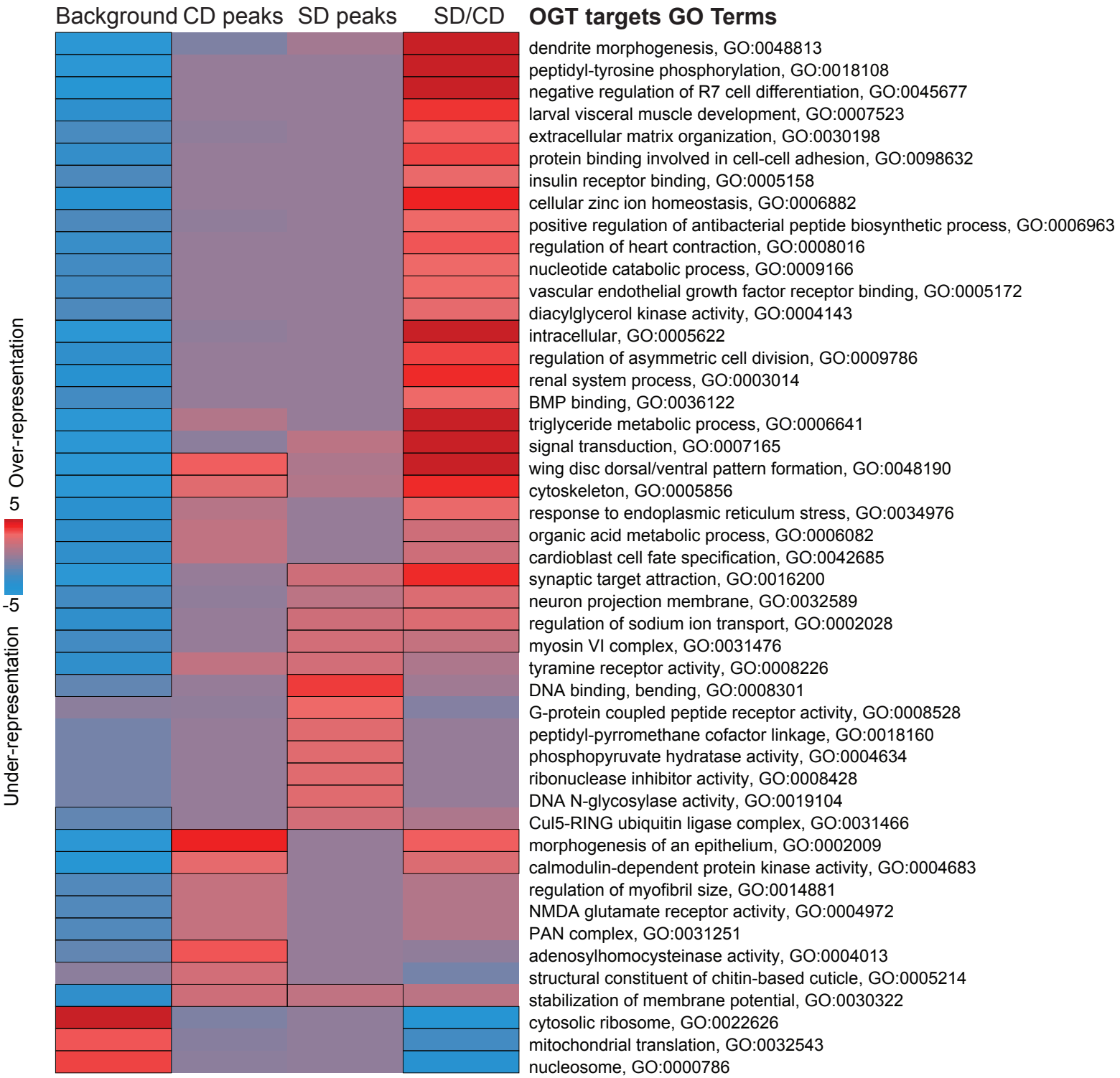
Background
CD peaks
SD peaks
SD/CD
OGT targets GO Terms
dendrite morphogenesis, GO:0048813
peptidyl-tyrosine phosphorylation, GO:0018108
negative regulation of R7 cell differentiation, GO:0045677
larval visceral muscle development, GO:0007523
extracellular matrix organization, GO:0030198
protein binding involved in cell-cell adhesion, GO:0098632
insulin receptor binding, GO:0005158
cellular zinc ion homeostasis, GO:0006882
positive regulation of antibacterial peptide biosynthetic process, GO:0006963
regulation of heart contraction, GO:0008016
nucleotide catabolic process, GO:0009166
vascular endothelial growth factor receptor binding, GO:0005172
diacylglycerol kinase activity, GO:0004143
intracellular, GO:0005622
regulation of asymmetric cell division, GO:0009786
renal system process, GO:0003014
BMP binding, GO:0036122
triglyceride metabolic process, GO:0006641
signal transduction, GO:0007165
wing disc dorsal/ventral pattern formation, GO:0048190
cytoskeleton, GO:0005856
response to endoplasmic reticulum stress, GO:0034976
organic acid metabolic process, GO:0006082
cardioblast cell fate specification, GO:0042685
synaptic target attraction, GO:0016200
neuron projection membrane, GO:0032589
regulation of sodium ion transport, GO:0002028
myosin VI complex, GO:0031476
tyramine receptor activity, GO:0008226
DNA binding, bending, GO:0008301
G-protein coupled peptide receptor activity, GO:0008528
peptidyl-pyrromethane cofactor linkage, GO:0018160
phosphopyruvate hydratase activity, GO:0004634
ribonuclease inhibitor activity, GO:0008428
DNA N-glycosylase activity, GO:0019104
Cul5-RING ubiquitin ligase complex, GO:0031466
morphogenesis of an epithelium, GO:0002009
calmodulin-dependent protein kinase activity, GO:0004683
regulation of myofibril size, GO:0014881
NMDA glutamate receptor activity, GO:0004972
PAN complex, GO:0031251
adenosylhomocysteinase activity, GO:0004013
structural constituent of chitin-based cuticle, GO:0005214
stabilization of membrane potential, GO:0030322
cytosolic ribosome, GO:0022626
mitochondrial translation, GO:0032543
nucleosome, GO:0000786
Over-representation
5
-5
Under-representation

870 **Figure S2- Related to Figure 1, Pathway enrichment analysis of OGT chromatin targets in**
871 **the *Gr5a*+ neurons**

872 iPAGE identification of pathways depleted (blue) or enriched (red) compared to background gene
873 list from the *OGT::Dam* peaks on a control, sugar, and difference of sugar/control diet. The scale
874 represents over-representation (red) or under-representation (blue) of genes within a specific bin
875 for the corresponding GO term. Black outlined boxes represent $q<0.05$.

Sung Vaziri
Supplemental 3

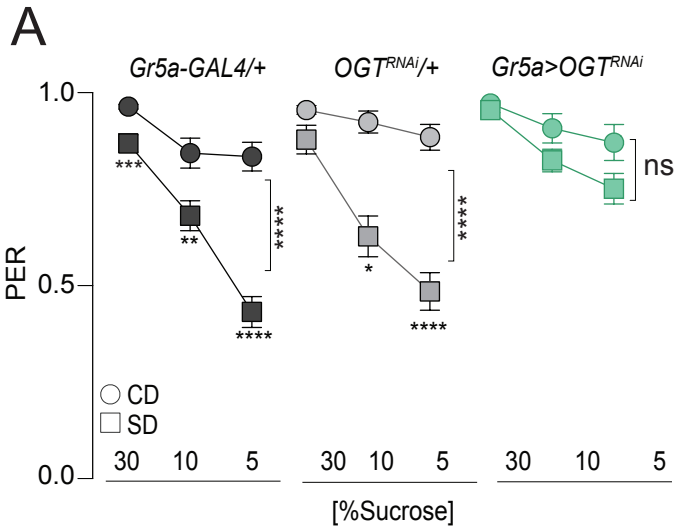

876 **Figure S3- Related to Figure 3, OSMI treatment phenocopies OGT KD in the Gr5a+ neurons.**

877 Taste responses (*y-axis*) to stimulation of the labellum with 30, 10, and 5% sucrose (*x-axis*) in
878 flies with knockdown of OGT (green) or controls (shades of gray) in flies fed a CD (circles) or SD
879 (squares). n=18-51. Two way repeated measure ANOVA, main effect of genotype: *Gr5a>wcs*
880 *p<0.0001* (Tukey multiple comparison 30% *p=0.0008*, 10% *p=0.0047*, 5% *p<0.0001*), *Gr5a>OGT-*
881 *RNAi p=0.2657* (Sidak multiple comparison 30% *p=0.2792*, 10% *p=0.9756*, 5% *p=0.4883*), *OGT-*
882 *RNAi>wcs* (Sidak multiple comparison 30% *p=0.5923*, 10% *p=0.0381*, 5% *p<0.0001*).

Sung Vaziri

Supplement 4

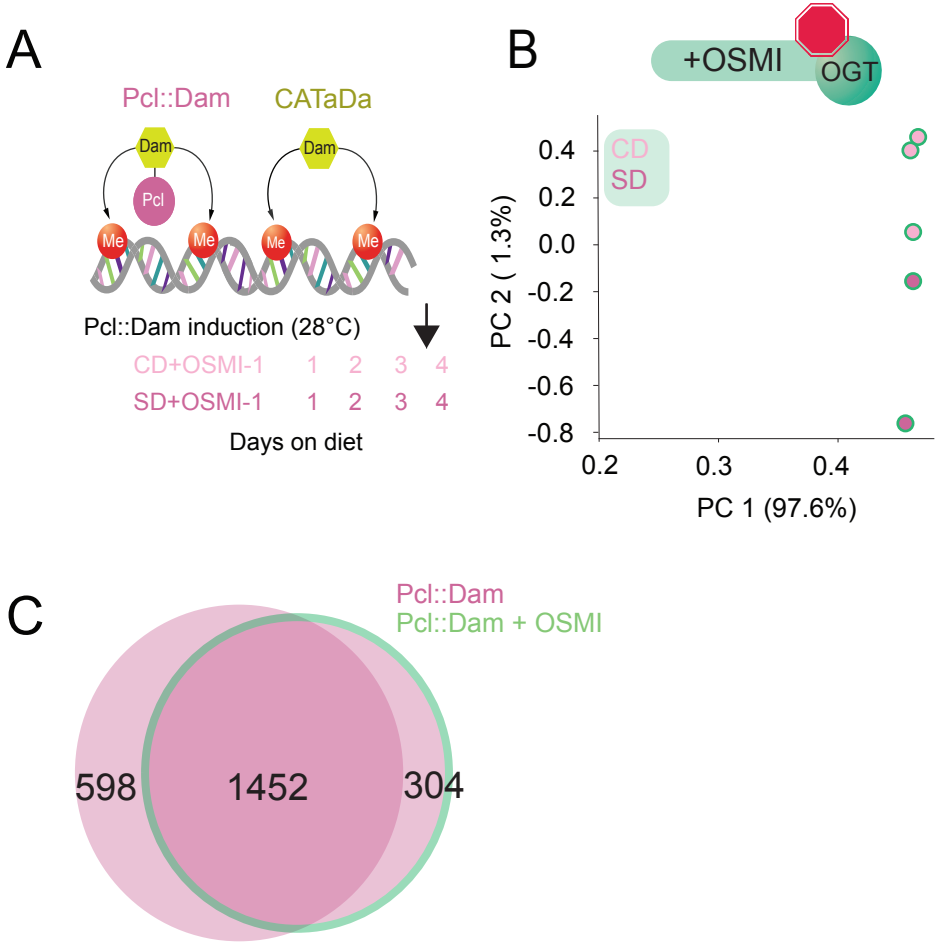

883 **Figure S4- Related to Figure 3, Pcl occupancy at PRE and Pcl peaks with inhibition of OGT**
884 **activity.**

885 (A) Design of the TaDa and CaTaDa experiment in flies fed a CD+OSMI and SD + OSMI.
886 (B) Principal component analysis of normalized log2(*Pcl::Dam/Dam*) flies on CD+OSMI (light
887 pink) or SD+OSMI (dark pink).
888 (C) Overlap of log2(*Dam::Pcl/Dam*) chromatin occupancy peaks in flies with (green outline) or
889 without (pink) OSMI (find_peaks, $q<0.01$).

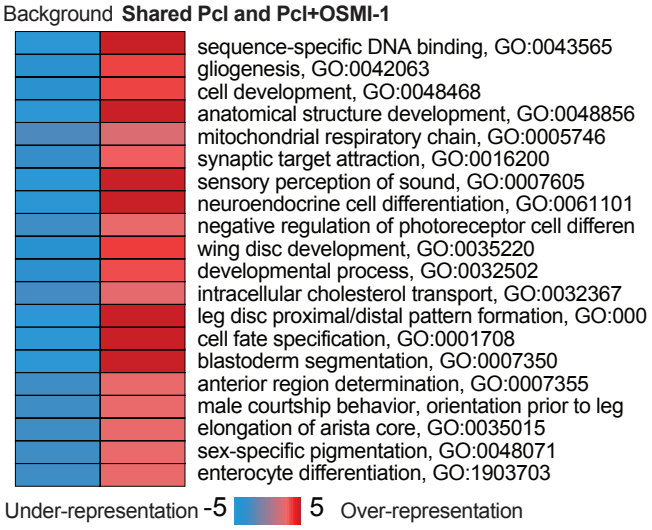
Background
Shared Pcl and Pcl+OSMI-1
sequence-specific DNA binding, GO:0043565
gliogenesis, GO:0042063
cell development, GO:0048468
anatomical structure development, GO:0048856
mitochondrial respiratory chain, GO:0005746
synaptic target attraction, GO:0016200
sensory perception of sound, GO:0007605
neuroendocrine cell differentiation, GO:0061101
negative regulation of photoreceptor cell differen
wing disc development, GO:0035220
developmental process, GO:0032502
intracellular cholesterol transport, GO:0032367
leg disc proximal/distal pattern formation, GO:000
cell fate specification, GO:0001708
blastoderm segmentation, GO:0007350
anterior region determination, GO:0007355
male courtship behavior, orientation prior to leg
elongation of arista core, GO:0035015
sex-specific pigmentation, GO:0048071
enterocyte differentiation, GO:1903703
Under-representation -5
5 Over-representation

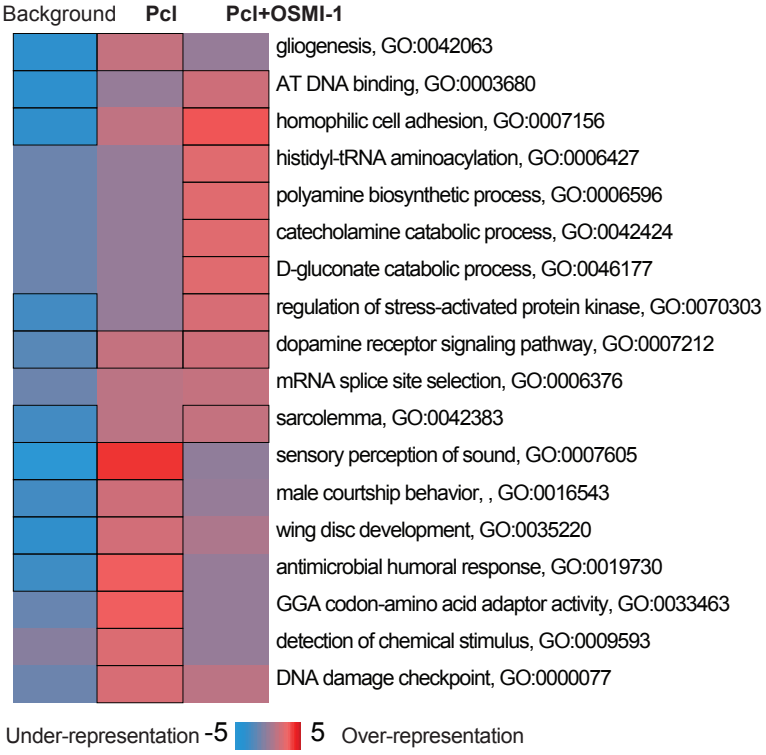
Background
Pcl
Pcl+OSMI-1
gliogenesis, GO:0042063
AT DNA binding, GO:0003680
homophilic cell adhesion, GO:0007156
histidyl-tRNA aminoacylation, GO:0006427
polyamine biosynthetic process, GO:0006596
catecholamine catabolic process, GO:0042424
D-gluconate catabolic process, GO:0046177
regulation of stress-activated protein kinase, GO:0070303
dopamine receptor signaling pathway, GO:0007212
mRNA splice site selection, GO:0006376
sarcolemma, GO:0042383
sensory perception of sound, GO:0007605
male courtship behavior, , GO:0016543
wing disc development, GO:0035220
antimicrobial humoral response, GO:0019730
GGA codon-amino acid adaptor activity, GO:0033463
detection of chemical stimulus, GO:0009593
DNA damage checkpoint, GO:0000077
Under-representation -5
5 Over-representation

890 **Figure S5- Related to Figure 3, Pathway enrichment analysis of the effects of OSMI on**
891 ***Dam::Pcl* peaks.**

892 iPAGE identification of pathways depleted (blue) or enriched (red) compared to background gene
893 list from the *Dam::Pcl* peaks shared (left) or different (right) between SD/CD with or without OSMI.
894 Scale represents over-representation (red) or under-representation (blue) of genes within a
895 specific bin for the corresponding GO term. Black outlined boxes represent $q<0.05$.

Sung Vaziri
Supplement 6

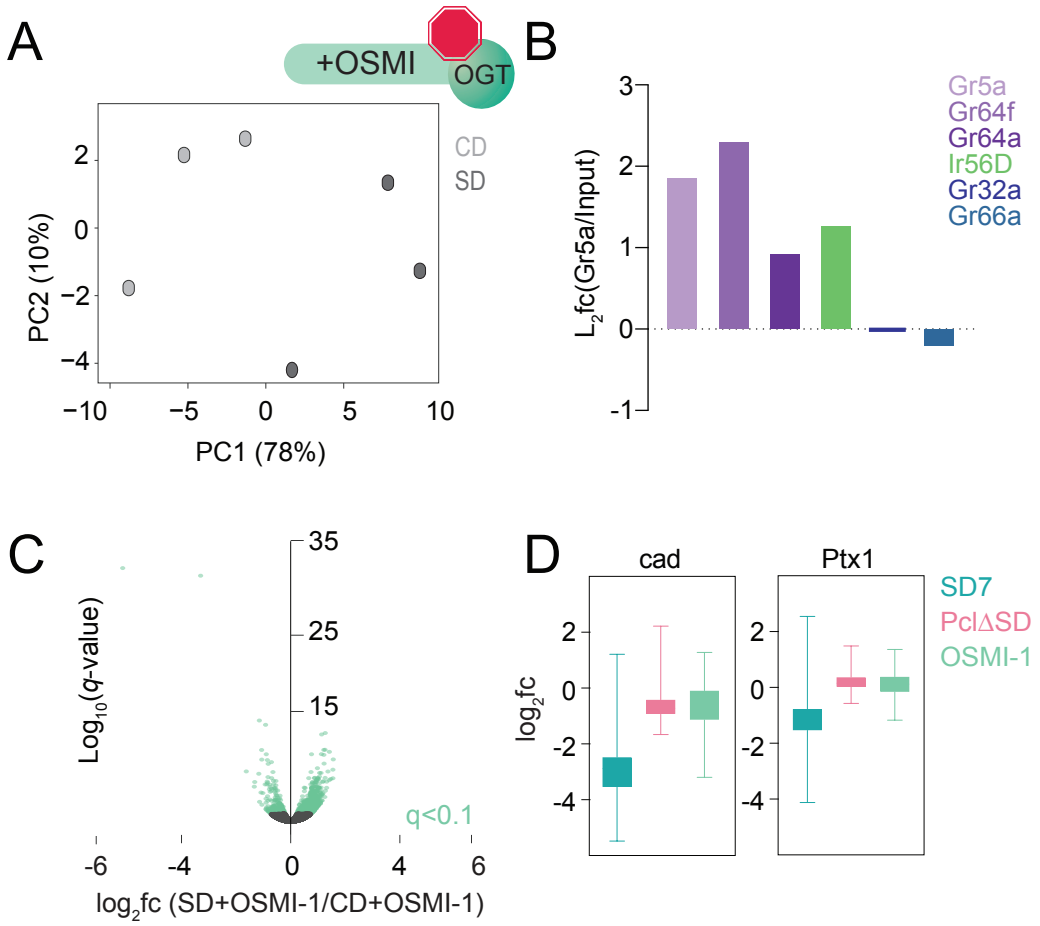

896 **Figure S6- Related to Figure 3, Transcriptional responses to the dietary environment when**
897 **OGT activity was inhibited.**

898 (A) Principal component analysis of *Gr5a > UAS-Rpl3-3XFLAG* flies on a control (light gray)
899 or sugar (dark gray) diet for 7 days supplemented with OSMI-1.
900 (B) Log_2fold change (l2fc) (Gr5a IP/Input) for *Gr5a, Gr64f, Gr64a, Ir56D, Gr32a, and Gr66a*
901 genes**.**
902 (C) Volcano plot representing differential expression in the *Gr5a*+ neurons of age-matched
903 male *Gr5a>UAS-Rpl3-3XFLAG* flies on a control or sugar diet for 7 days supplemented
904 with OSMI-1. *n*=3 replicates per condition. Genes with *q*<0.1 (Wald test) are in green.
905 (D) Log_2fold change (l2fc) for candidate gene targets of *Cad* and *Ptx1* at SD7 (teal), Pcl^{c429}
906 *(pink),* and OSMI-1 fed flies at SD7 (green).

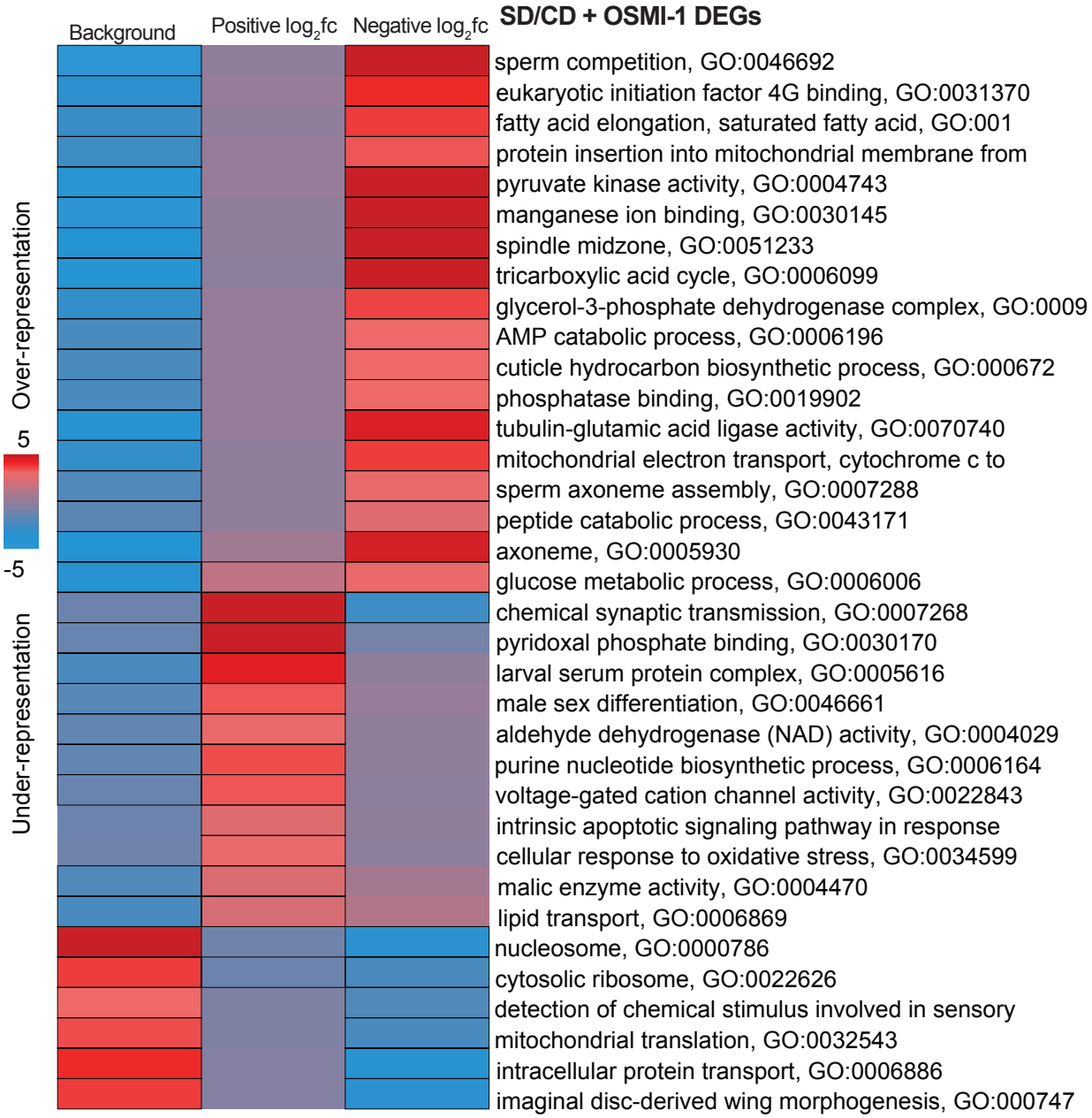
SD/CD + OSMI-1 DEGs
Background
Positive log2fc
Negative log2fc
Over-representation
5
-5
Under-representation
sperm competition, GO:0046692
eukaryotic initiation factor 4G binding, GO:0031370
fatty acid elongation, saturated fatty acid, GO:001
protein insertion into mitochondrial membrane from
pyruvate kinase activity, GO:0004743
manganese ion binding, GO:0030145
spindle midzone, GO:0051233
tricarboxylic acid cycle, GO:0006099
glycerol-3-phosphate dehydrogenase complex, GO:0009
AMP catabolic process, GO:0006196
cuticle hydrocarbon biosynthetic process, GO:000672
phosphatase binding, GO:0019902
tubulin-glutamic acid ligase activity, GO:0070740
mitochondrial electron transport, cytochrome c to
sperm axoneme assembly, GO:0007288
peptide catabolic process, GO:0043171
axoneme, GO:0005930
glucose metabolic process, GO:0006006
chemical synaptic transmission, GO:0007268
pyridoxal phosphate binding, GO:0030170
larval serum protein complex, GO:0005616
male sex differentiation, GO:0046661
aldehyde dehydrogenase (NAD) activity, GO:0004029
purine nucleotide biosynthetic process, GO:0006164
voltage-gated cation channel activity, GO:0022843
intrinsic apoptotic signaling pathway in response
cellular response to oxidative stress, GO:0034599
malic enzyme activity, GO:0004470
lipid transport, GO:0006869
nucleosome, GO:0000786
cytosolic ribosome, GO:0022626
detection of chemical stimulus involved in sensory
mitochondrial translation, GO:0032543
intracellular protein transport, GO:0006886
imaginal disc-derived wing morphogenesis, GO:000747

907 **Figure S7- Related to Figure 3, Pathway enrichment analysis of genes reverted or**
908 **unchanged by OSMI.**

909 iPAGE identification of pathways depleted (blue) or enriched (red) compared to background gene
910 list from genes with positive or negative log2 fold changes on SD+OSMI-1. Scale represents over-
911 representation (red) or under-representation (blue) of genes within a specific bin for the
912 corresponding GO term. Black outlined boxes represent $q<0.05$.

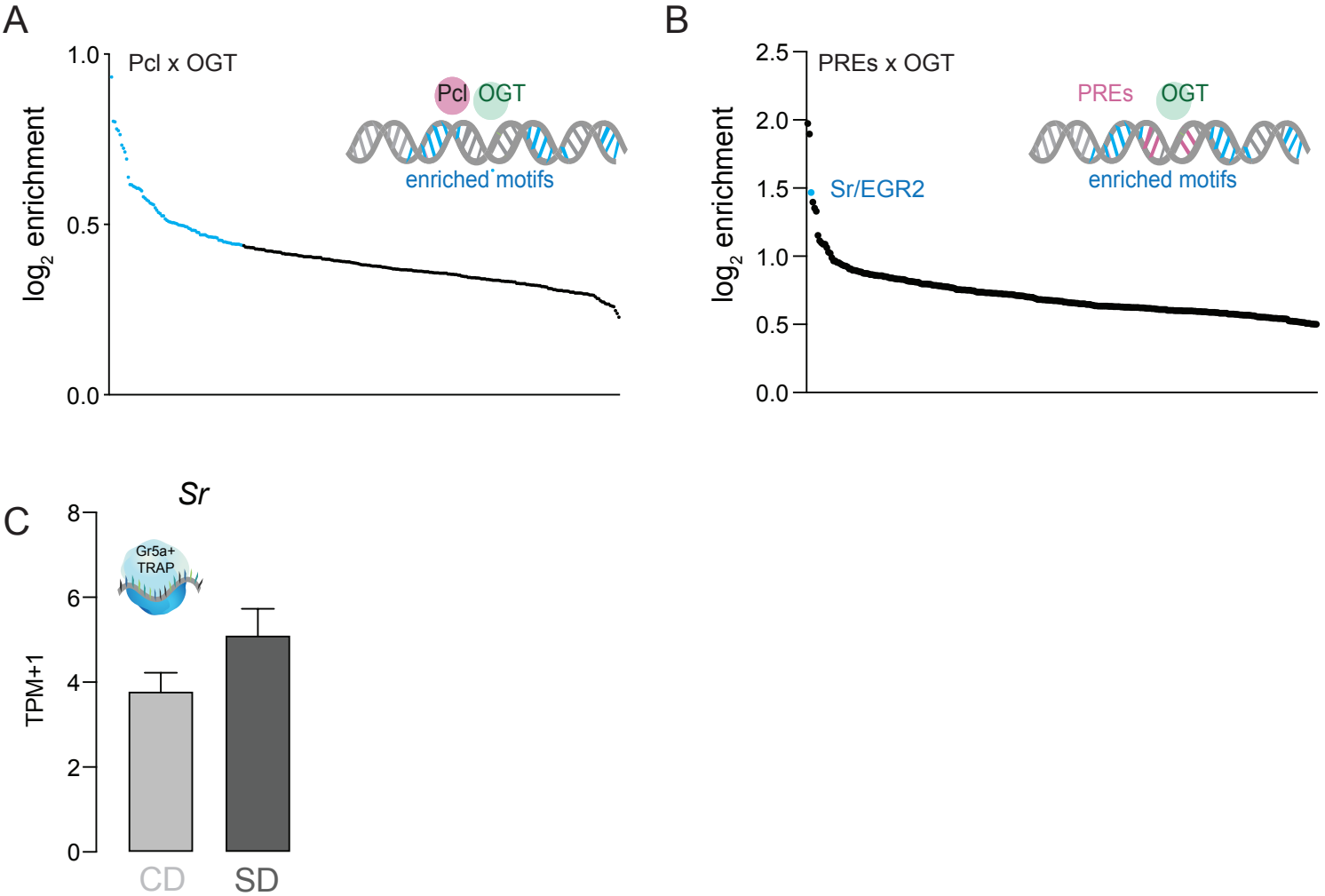
A
Pcl x OGT
log2 enrichment
1.0
0.5
0.0
Pcl
OGT
enriched motifs
B
PREs x OGT
log2 enrichment
2.5
2.0
1.5
1.0
0.5
0.0
Sr/EGR2
PREs
OGT
enriched motifs
C
Sr
TPM+1
8
6
4
2
0
Gr5a+
TRAP
CD
SD

913 **Figure S8: Related to Figure 4, Enrichment analysis of cis-regulatory sites present in OGT**
914 **and PREs.**

915 (A) Log_2fold enrichment of TF cis-regulatory sites found at OGT + Pcl; blue $q<0.01$.
916 (B) Log_2fold enrichment of TF cis-regulatory sites found at OGT + PREs.

917 (C) *Sr* mRNA reads normalized as transcripts per million (TPMs) in the Gr5a+ neurons of flies
918 on a CD (light gray) or SD (dark gray) for 7 days, $q>0.01$.

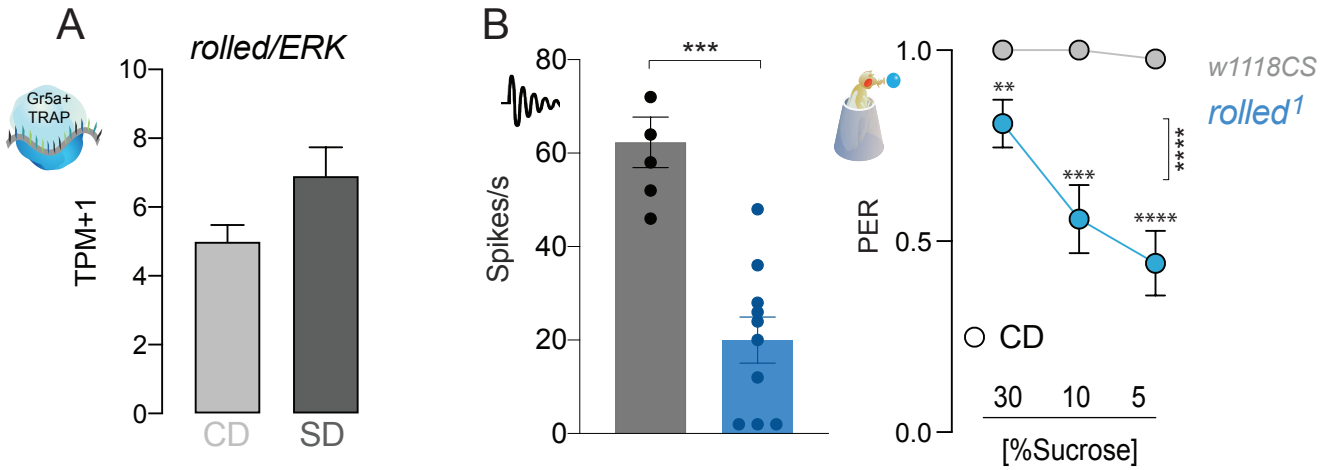
A
rolled/ERK
Gr5a+
TRAP
TPM+1
10
8
6
4
2
0
CD
SD
B
Spikes/s
80
60
40
20
0
***
PER
1.0
0.5
0.0
**
***
****
****
w1118CS
rolled1
CD
30
10
5
[%Sucrose]

919 **Figure S9: Related to Figure 5, *rl*/ERK is required for taste responses to sugar**

920 (A) *rl* RNA reads normalized as transcripts per million (TPMs) in the Gr5a+ neurons of flies
921 on a CD (light gray) or SD (dark gray) for 7 days. $q>0.01$.
922 (B) (*left*) Averaged neuronal responses to 25 mM sucrose from L-type sensilla in *rl* mutant
923 (blue) and control (gray) flies. n=6-10. Mann-Whitney test: p=0.0005. (*right*) Taste
924 responses (*y-axis*) to stimulation of the labellum with 30, 10, and 5% sucrose (*x-axis*) in *rl*
925 mutant and control flies fed a CD. n=26. Two way repeated measure ANOVA, main effect
926 of genotype $p<0.0001$; Dunn's post-test $^{**}p < 0.01$ and $^{***}p<0.001$ vs controls.
927

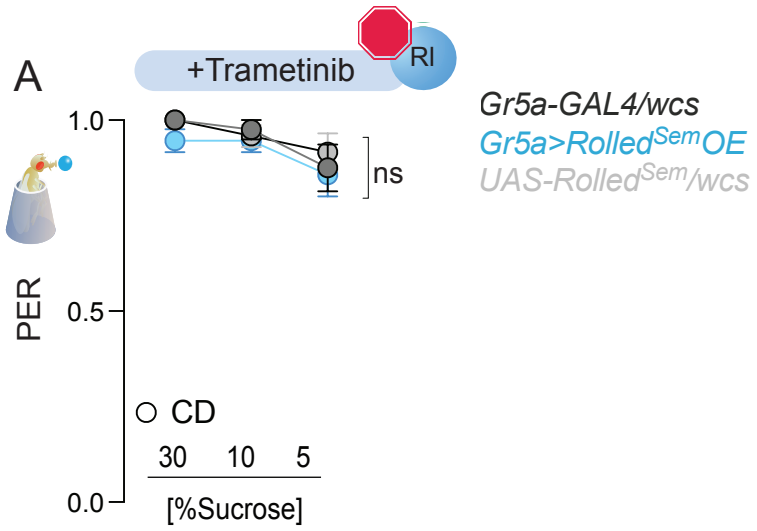
A
+Trametinib
RI
Gr5a-GAL4/wcs
Gr5a>Rolled^Sem OE
UAS-Rolled^Sem/wcs
1.0
0.5
0.0
PER
ns
CD
30 10 5
[%Sucrose]

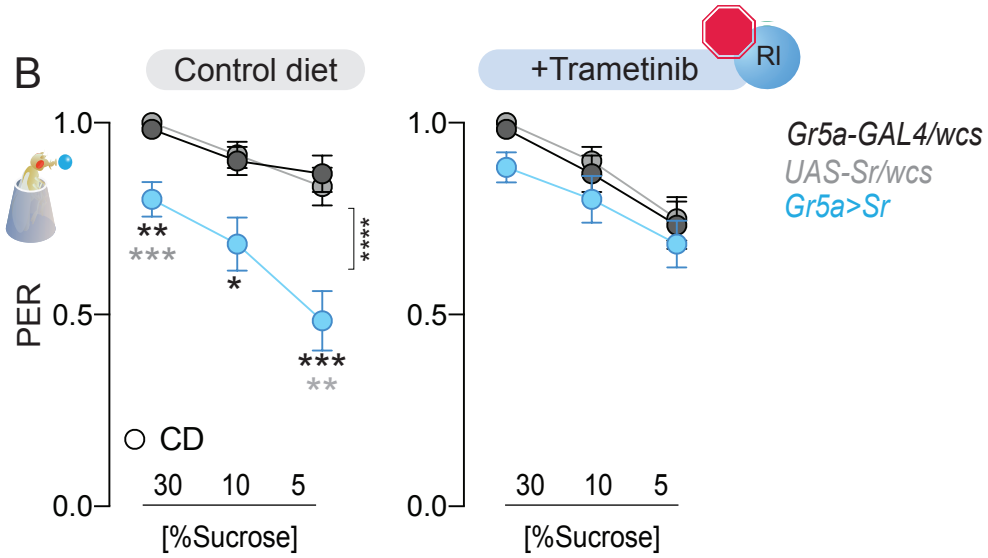
B
Control diet
+Trametinib
RI
Gr5a-GAL4/wcs
UAS-Sr/wcs
Gr5a>Sr
1.0
0.5
0.0
PER
**
***
*
***
**
****
CD
30 10 5
[%Sucrose]

928 **Figure S10, related to Figure 6: Effects of ERK inhibitor Trametinib on genetic**
929 **manipulations of *Sr* and *rl* levels.**

930 (A) Taste responses (*y-axis*) to stimulation of the labellum with 30, 10, and 5% sucrose (*x-*
931 *axis*) in flies fed a CD+Trametinib (blue) and with overexpression of *rl* (blue or controls in
932 gray) n=24-28. Two-way repeated measure ANOVA, main effect of genotype *p=0.0206*
933 and genotype x concentration *p=0.3671*.
934 (B) Taste responses (*y-axis*) to stimulation of the labellum with 30, 10, and 5% sucrose (*x-*
935 *axis*) in flies fed a CD with or without Trametinib (blue) and with overexpression of *Sr* (blue,
936 or controls in gray) n=22-38. CD: Two-way repeated measure ANOVA main effect of
937 genotype *p<0.0001* and genotype x concentration *p=0.0037* with Sidak multiple
938 comparison tests, 3*0% p=0.0012, 10% p=0.0002, 5% p<0.0001*; Trametinib: Two way
939 repeated measure ANOVA main effect of genotype *p=0.2192.*

940 **REFERENCES**

941 Anders S, Pyl PT, Huber W. 2015. HTSeq--a Python framework to work with high-throughput
942 sequencing data. *Bioinformatics* **31**:166–169.
943 Andrews S, Others. 2010. FastQC: a quality control tool for high throughput sequence data.
944 Ardiel EL, McDiarmid TA, Timbers TA, Lee KCY, Safaei J, Pelech SL, Rankin CH. 2018. CaMK
945 (CMK-1) and O-GlcNAc transferase (OGT-1) modulate mechanosensory responding and
946 habituation in an interstimulus interval-dependent manner in Caenorhabditis elegans.
947 *bioRxiv*. doi:10.1101/115972
948 Ballaré C, Lange M, Lapinaite A, Martin GM, Morey L, Pascual G, Liefke R, Simon B, Shi Y,
949 Gozani O, Carlomagno T, Benitah SA, Di Croce L. 2012. Phf19 links methylated Lys36 of
950 histone H3 to regulation of Polycomb activity. *Nat Struct Mol Biol* **19**:1257–1265.
951 Beckmann AM, Wilce PA. 1997. Egr transcription factors in the nervous system. *Neurochem Int*
952 **31**:477–510; discussion 517–6.
953 Benjamini Y, Hochberg Y. 1995. Controlling the False Discovery Rate: A Practical and Powerful
954 Approach to Multiple Testing. *J R Stat Soc Series B Stat Methodol* **57**:289–300.
955 Biggs WH 3rd, Zavitz KH, Dickson B, van der Straten A, Brunner D, Hafen E, Zipursky SL.
956 1994. The Drosophila rolled locus encodes a MAP kinase required in the sevenless signal
957 transduction pathway. *EMBO J* **13**:1628–1635.
958 Bouché C, Serdy S, Kahn CR, Goldfine AB. 2004. The cellular fate of glucose and its relevance
959 in type 2 diabetes. *Endocr Rev* **25**:807–830.
960 Brien GL, Gambero G, O'Connell DJ, Jerman E, Turner SA, Egan CM, Dunne EJ, Jurgens MC,
961 Wynne K, Piao L, Lohan AJ, Ferguson N, Shi X, Sinha KM, Loftus BJ, Cagney G, Bracken
962 AP. 2012. Polycomb PHF19 binds H3K36me3 and recruits PRC2 and demethylase NO66
963 to embryonic stem cell genes during differentiation. *Nat Struct Mol Biol* **19**:1273–1281.
964 Butler AA, Sanchez RG, Jarome TJ, Webb WM, Lubin FD. 2019. O-GlcNAc and EZH2-
965 mediated epigenetic regulation of gene expression during consolidation of fear memories.
966 *Learn Mem* **26**:373–379.
967 Cai L, Rothbart SB, Lu R, Xu B, Chen W-Y, Tripathy A, Rockowitz S, Zheng D, Patel DJ, Allis
968 CD, Strahl BD, Song J, Wang GG. 2013. An H3K36 methylation-engaging Tudor motif of
969 polycomb-like proteins mediates PRC2 complex targeting. *Mol Cell* **49**:571–582.
970 Castillo-Quan JI, Tain LS, Kinghorn KJ, Li L, Grönke S, Hinze Y, Blackwell TK, Bjedov I,
971 Partridge L. 2019. A triple drug combination targeting components of the nutrient-sensing
972 network maximizes longevity. *Proc Natl Acad Sci U S A* **116**:20817–20819.

973 Chen X, Dickman D. 2017. Development of a tissue-specific ribosome profiling approach in
974 Drosophila enables genome-wide evaluation of translational adaptations. *PLoS Genet*
975 **13**:e1007117.
976 Chen X, Rahman R, Guo F, Rosbash M. 2016. Genome-wide identification of neuronal activity-
977 regulated genes in Drosophila. *Elife* **5**. doi:10.7554/eLife.19942
978 Chu C-S, Lo P-W, Yeh Y-H, Hsu P-H, Peng S-H, Teng Y-C, Kang M-L, Wong C-H, Juan L-J.
979 2014. O-GlcNAcylation regulates EZH2 protein stability and function. *Proc Natl Acad Sci U*
980 *S A* **111**:1355–1360.
981 Chyb S, Dahanukar A, Wickens A, Carlson JR. 2003. Drosophila Gr5a encodes a taste receptor
982 tuned to trehalose. *Proc Natl Acad Sci U S A* **100 Suppl 2**:14526–14530.
983 Cork GK, Tan EP, Thompson J, McGreal S, Machecek M, Kelsh J, Peterson K, Apte U,
984 Slawson C. 2018. Sustained O-GlcNAcylation amplifies erk signaling. *FASEB J* **32**.
985 doi:10.1096/fasebj.2018.32.1_supplement.673.20
986 Dai Z, Ramesh V, Locasale JW. 2020. The evolving metabolic landscape of chromatin biology
987 and epigenetics. *Nat Rev Genet* **21**:737–753.
988 DeBerardinis RJ, Chandel NS. 2016. Fundamentals of cancer metabolism. *Sci Adv* **2**:e1600200.
989 Decourcelle A, Very N, Djouina M, Loison I, Thévenet J, Body-Malapel M, Lelièvre E, Coqueret
990 O, Leprince D, El Yazidi-Belkoura I, Dehennaut V. 2020. O-GlcNAcylation Links Nutrition to
991 the Epigenetic Downregulation of UNC5A during Colon Carcinogenesis. *Cancers* **12**.
992 doi:10.3390/cancers12113168
993 Delventhal R, Kiely A, Carlson JR. 2014. Electrophysiological recording from Drosophila labellar
994 taste sensilla. *J Vis Exp* e51355.
995 Dobin A, Davis CA, Schlesinger F, Drenkow J, Zaleski C, Jha S, Batut P, Chaisson M, Gingeras
996 TR. 2013. STAR: ultrafast universal RNA-seq aligner. *Bioinformatics* **29**:15–21.
997 Duclot F, Kabbaj M. 2017. The Role of Early Growth Response 1 (EGR1) in Brain Plasticity and
998 Neuropsychiatric Disorders. *Front Behav Neurosci* **11**:35.
999 Fabris F. 2009. Shannon information theory and molecular biology. *J Interdiscip Math* **12**:41–87.
1000 Faubert B, Solmonson A, DeBerardinis RJ. 2020. Metabolic reprogramming and cancer
1001 progression. *Science* **368**. doi:10.1126/science.aaw5473
1002 Filion GJ, van Bemmel JG, Braunschweig U, Talhout W, Kind J, Ward LD, Brugman W, de
1003 Castro IJ, Kerkhoven RM, Bussemaker HJ, van Steensel B. 2010. Systematic protein
1004 location mapping reveals five principal chromatin types in Drosophila cells. *Cell* **143**:212–
1005 224.
1006 Floridi L. 2005. Is semantic information meaningful data? *Philos Phenomenol Res* **70**:351–370.

1007 Forma E, Jóźwiak P, Ciesielski P, Zaczek A, Starska K, Bryś M, Krześlak A. 2018. Impact of
1008 OGT deregulation on EZH2 target genes FOXA1 and FOXC1 expression in breast cancer
1009 cells. *PLoS One* **13**:e0198351.
1010 Gambetta MC, Müller J. 2015. A critical perspective of the diverse roles of O-GlcNAc
1011 transferase in chromatin. *Chromosoma* **124**:429–442.
1012 Gambetta MC, Müller J. 2014. O-GlcNAcylation prevents aggregation of the Polycomb group
1013 repressor polyhomeotic. *Dev Cell* **31**:629–639.
1014 Gambetta MC, Oktaba K, Müller J. 2009. Essential role of the glycosyltransferase sxc/Ogt in
1015 polycomb repression. *Science* **325**:93–96.
1016 Ganguly A, Dey M, Scott C, Duong V-K, Dahanukar A. 2021. Dietary Macronutrient Imbalances
1017 Lead to Compensatory Changes in Peripheral Taste via Independent Signaling Pathways. *J*
1018 *Neurosci*. doi:10.1523/JNEUROSCI.2154-20.2021
1019 Gao J, Yang Y, Qiu R, Zhang K, Teng X, Liu R, Wang Y. 2018. Proteomic analysis of the OGT
1020 interactome: novel links to epithelial–mesenchymal transition and metastasis of cervical
1021 cancer. *Carcinogenesis* **39**:1222–1234.
1022 Giles AC, Desbois M, Opperman KJ, Tavora R, Maroni MJ, Grill B. 2019. A complex containing
1023 the O-GlcNAc transferase OGT-1 and the ubiquitin ligase EEL-1 regulates GABA neuron
1024 function. *J Biol Chem* **294**:6843–6856.
1025 Gonzales BJ, Mukherjee D, Ashwal-Fluss R, Loewenstein Y, Citri A. 2020. Subregion-specific
1026 rules govern the distribution of neuronal immediate-early gene induction. *Proc Natl Acad*
1027 *Sci U S A* **117**:23304–23310.
1028 Goodarzi H, Elemento O, Tavazoie S. 2009. Revealing global regulatory perturbations across
1029 human cancers. *Mol Cell* **36**:900–911.
1030 Hanover JA, Krause MW, Love DC. 2010. The hexosamine signaling pathway: O-GlcNAc
1031 cycling in feast or famine. *Biochim Biophys Acta* **1800**:80–95.
1032 Hardivillé S, Hart GW. 2014. Nutrient regulation of signaling, transcription, and cell physiology
1033 by O-GlcNAcylation. *Cell Metab* **20**:208–213.
1034 Hart GW. 2019. Nutrient regulation of signaling and transcription. *J Biol Chem* **294**:2211–2231.
1035 Hart GW, Slawson C, Ramirez-Correa G, Lagerlof O. 2011. Cross talk between O-
1036 GlcNAcylation and phosphorylation: roles in signaling, transcription, and chronic disease.
1037 *Annu Rev Biochem* **80**:825–858.
1038 Hawkins M, Barzilai N, Liu R, Hu M, Chen W, Rossetti L. 1997. Role of the glucosamine
1039 pathway in fat-induced insulin resistance. *J Clin Invest* **99**:2173–2182.
1040 Heinz S, Benner C, Spann N, Bertolino E, Lin YC, Laslo P, Cheng JX, Murre C, Singh H, Glass

1041 CK. 2010. Simple combinations of lineage-determining transcription factors prime cis-
1042 regulatory elements required for macrophage and B cell identities. *Mol Cell* **38**:576–589.
1043 Hirosawa M, Laboratory of Cellular Biochemistry, Department of Animal Resource
1044 Sciences/Veterinary Medical Sciences, The University of Tokyo, Tokyo 113-8657, Japan,
1045 Hayakawa K, Shiota K, Tanaka S, Laboratory of Cellular Biochemistry, Department of
1046 Animal Resource Sciences/Veterinary Medical Sciences, The University of Tokyo, Tokyo
1047 113-8657, Japan, Waseda Research Institute for Science and Engineering, Waseda
1048 University, Tokyo 169-8555, Japan, Laboratory of Cellular Biochemistry, Department of
1049 Animal Resource Sciences/Veterinary Medical Sciences, The University of Tokyo, Tokyo
1050 113-8657, Japan. 2018. Histone O-GlcNAcylation and potential biological functions. *OBM*
1051 *genet* **2**:1–1.
1052 Hobert O. 2011. Regulation of terminal differentiation programs in the nervous system. *Annu*
1053 *Rev Cell Dev Biol* **27**:681–696.
1054 Huang Z, Cai L, Tu BP. 2015. Dietary control of chromatin. *Curr Opin Cell Biol* **34**:69–74.
1055 Hwang H, Rhim H. 2019. Acutely elevated O-GlcNAcylation suppresses hippocampal activity by
1056 modulating both intrinsic and synaptic excitability factors. *Sci Rep* **9**:7287.
1057 Jiang M, Qiu Z, Zhang S, Fan X, Cai X, Xu B, Li X, Zhou J, Zhang X, Chu Y, Wang W, Liang J,
1058 Horvath T, Yang X, Wu K, Nie Y, Fan D. 2016. Elevated O-GlcNAcylation promotes gastric
1059 cancer cells proliferation by modulating cell cycle related proteins and ERK 1/2 signaling.
1060 *Oncotarget* **7**:61390–61402.
1061 Jiang M, Xu B, Li X, Shang Y, Chu Y, Wang W, Chen D, Wu N, Hu S, Zhang S, Li M, Wu K,
1062 Yang X, Liang J, Nie Y, Fan D. 2019. O-GlcNAcylation promotes colorectal cancer
1063 metastasis via the miR-101-O-GlcNAc/EZH2 regulatory feedback circuit. *Oncogene*
1064 **38**:301–316.
1065 Katada S, Imhof A, Sassone-Corsi P. 2012. Connecting threads: epigenetics and metabolism.
1066 *Cell* **148**:24–28.
1067 Konzman D, Abramowitz LK, Steenackers A, Mukherjee MM, Na H-J, Hanover JA. 2020. O-
1068 GlcNAc: Regulator of Signaling and Epigenetics Linked to X-linked Intellectual Disability.
1069 *Front Genet* **11**:605263.
1070 Lagerlöf O, Hart GW, Huganir RL. 2017. O-GlcNAc transferase regulates excitatory synapse
1071 maturity. *Proc Natl Acad Sci U S A* **114**:1684–1689.
1072 Lagerlöf O, Slocomb JE, Hong I, Aponte Y, Blackshaw S, Hart GW, Huganir RL. 2016. The
1073 nutrient sensor OGT in PVN neurons regulates feeding. *Science* **351**:1293–1296.
1074 Langmead B, Salzberg SL. 2012. Fast gapped-read alignment with Bowtie 2. *Nat Methods*

1075 **9**:357–359.
1076 Lavoie H, Gagnon J, Therrien M. 2020. ERK signalling: a master regulator of cell behaviour, life
1077 and fate. *Nat Rev Mol Cell Biol* **21**:607–632.
1078 Lei Y, Chen T, Li Y, Shang M, Zhang Y, Jin Y, Yu Q, Guo F, Wang T. 2020. O-GlcNAcylation of
1079 PFKFB3 is required for tumor cell proliferation under hypoxia. *Oncogenesis* **9**:21.
1080 Liu H, Chen Y-G. 2022. The Interplay Between TGF-β Signaling and Cell Metabolism. *Front Cell*
1081 *Dev Biol* **10**:846723.
1082 Li YH, Liu X, Vanselow JT, Zheng H, Schlosser A, Chiu JC. 2019. O-GlcNAcylation of PERIOD
1083 regulates its interaction with CLOCK and timing of circadian transcriptional repression.
1084 *PLoS Genet* **15**:e1007953.
1085 Lo P-W, Shie J-J, Chen C-H, Wu C-Y, Hsu T-L, Wong C-H. 2018. O-GlcNAcylation regulates
1086 the stability and enzymatic activity of the histone methyltransferase EZH2. *Proc Natl Acad*
1087 *Sci U S A* **115**:7302–7307.
1088 Love MI, Huber W, Anders S. 2014. Moderated estimation of fold change and dispersion for
1089 RNA-seq data with DESeq2. *Genome Biol* **15**:550.
1090 Marder E, Prinz AA. 2002. Modeling stability in neuron and network function: the role of activity
1091 in homeostasis. *Bioessays* **24**:1145–1154.
1092 Marshall OJ, Brand AH. 2015. damidseq_pipeline: an automated pipeline for processing DamID
1093 sequencing datasets. *Bioinformatics* **31**:3371–3373.
1094 Marshall OJ, Southall TD, Cheetham SW, Brand AH. 2016. Cell-type-specific profiling of
1095 protein–DNA interactions without cell isolation using targeted DamID with next-generation
1096 sequencing. *Nat Protoc* **11**:1586–1598.
1097 Marshall S, Nadeau O, Yamasaki K. 2004. Dynamic actions of glucose and glucosamine on
1098 hexosamine biosynthesis in isolated adipocytes: differential effects on glucosamine 6-
1099 phosphate, UDP-N-acetylglucosamine, and ATP levels. *J Biol Chem* **279**:35313–35319.
1100 May CE, Dus M. 2021. Confection Confusion: Interplay Between Diet, Taste, and Nutrition.
1101 *Trends in Endocrinology & Metabolism*. doi:10.1016/j.tem.2020.11.011
1102 May CE, Rosander J, Gottfried J, Dennis E, Dus M. 2020. Dietary sugar inhibits satiation by
1103 decreasing the central processing of sweet taste. *Elife* **9**. doi:10.7554/eLife.54530
1104 May CE, Vaziri A, Lin YQ, Grushko O, Khabiri M, Wang Q-P, Holme KJ, Pletcher SD,
1105 Freddolino PL, Neely GG, Dus M. 2019. High Dietary Sugar Reshapes Sweet Taste to
1106 Promote Feeding Behavior in Drosophila melanogaster. *Cell Rep* **27**:1675–1685.e7.
1107 McCluskey LP, He L, Dong G, Harris R. 2020. Chronic exposure to liquid sucrose and dry
1108 sucrose diet have differential effects on peripheral taste responses in female rats. *Appetite*

1109 **145**:104499.
1110 Miningou N, Blackwell KT. 2020. The road to ERK activation: Do neurons take alternate routes?
1111 *Cell Signal* **68**:109541.
1112 Müller M, Kersten S. 2003. Nutrigenomics: goals and strategies. *Nat Rev Genet* **4**:315–322.
1113 Murphy P, Davidson DR, Hill RE. 1989. Segment-specific expression of a homoeobox-
1114 containing gene in the mouse hindbrain. *Nature* **341**:156–159.
1115 Musselman LP, Kühnlein RP. 2018. Drosophila as a model to study obesity and metabolic
1116 disease. *J Exp Biol* **221**. doi:10.1242/jeb.163881
1117 Na J, Musselman LP, Pendse J, Baranski TJ, Bodmer R, Ocorr K, Cagan R. 2013. A Drosophila
1118 Model of High Sugar Diet-Induced Cardiomyopathy. *PLoS Genetics*.
1119 doi:10.1371/journal.pgen.1003175
1120 Na J, Sweetwyne MT, Park ASD, Susztak K, Cagan RL. 2015. Diet-Induced Podocyte
1121 Dysfunction in Drosophila and Mammals. *Cell Rep* **12**:636–647.
1122 Oellers N, Hafen E. 1996. Biochemical characterization of rolledSem, an activated form of
1123 Drosophila mitogen-activated protein kinase. *J Biol Chem* **271**:24939–24944.
1124 Olivier-Van Stichelen S, Hanover JA. 2015. You are what you eat: O-linked N-
1125 acetylglucosamine in disease, development and epigenetics. *Curr Opin Clin Nutr Metab*
1126 *Care* **18**:339–345.
1127 Olivier-Van Stichelen S, Wang P, Comly M, Love DC, Hanover JA. 2017. Nutrient-driven O-
1128 linked N-acetylglucosamine (O-GlcNAc) cycling impacts neurodevelopmental timing and
1129 metabolism. *J Biol Chem* **292**:6076–6085.
1130 Ortiz-Meoz RF, Jiang J, Lazarus MB, Orman M, Janetzko J, Fan C, Duveau DY, Tan Z-W,
1131 Thomas CJ, Walker S. 2015. A small molecule that inhibits OGT activity in cells. *ACS*
1132 *Chem Biol* **10**:1392–1397.
1133 Papa S, Choy PM, Bubici C. 2019. The ERK and JNK pathways in the regulation of metabolic
1134 reprogramming. *Oncogene* **38**:2223–2240.
1135 Parrish JZ, Kim CC, Tang L, Bergquist S, Wang T, Derisi JL, Jan LY, Jan YN, Davis GW. 2014.
1136 Krüppel mediates the selective rebalancing of ion channel expression. *Neuron* **82**:537–544.
1137 Quinlan AR, Hall IM. 2010. BEDTools: a flexible suite of utilities for comparing genomic
1138 features. *Bioinformatics* **26**:841–842.
1139 Ramírez F, Ryan DP, Grüning B, Bhardwaj V, Kilpert F, Richter AS, Heyne S, Dündar F, Manke
1140 T. 2016. deepTools2: a next generation web server for deep-sequencing data analysis.
1141 *Nucleic Acids Res* **44**:W160–5.
1142 Reed DR, Alhadeff AL, Beauchamp GK, Chaudhari N, Duffy VB, Dus M, Fontanini A,

1143 Glendinning JI, Green BG, Joseph PV, Kyriazis GA, Lyte M, Maruvada P, McGann JP,
1144 McLaughlin JT, Moran TH, Murphy C, Noble EE, Pepino MY, Pluznick JL, Rother KI, Saez
1145 E, Spector AC, Sternini C, Mattes RD. 2020. NIH Workshop Report: sensory nutrition and
1146 disease. *Am J Clin Nutr*. doi:10.1093/ajcn/nqaa302
1147 Reinagel P. 2000. Information theory in the brain. *Curr Biol* **10**:R542–4.
1148 Robles-Flores M, Moreno-Londoño AP, Castañeda-Patlán MC. 2021. Signaling Pathways
1149 Involved in Nutrient Sensing Control in Cancer Stem Cells: An Overview. *Front Endocrinol*
1150 **12**:627745.
1151 Ruan H-B, Dietrich MO, Liu Z-W, Zimmer MR, Li M-D, Singh JP, Zhang K, Yin R, Wu J, Horvath
1152 TL, Yang X. 2014. O-GlcNAc transferase enables AgRP neurons to suppress browning of
1153 white fat. *Cell* **159**:306–317.
1154 Sakabe K, Hart GW. 2010. O-GlcNAc Transferase Regulates Mitotic Chromatin Dynamics*. *J*
1155 *Biol Chem* **285**:34460–34468.
1156 Sarangi M, Dus M. 2021. Crème de la Créature: Dietary Influences on Behavior in Animal
1157 Models. *Frontiers in Behavioral Neuroscience; Lausanne*. doi:10.3389/fnbeh.2021.746299
1158 Sartor F, Donaldson LF, Markland DA, Loveday H, Jackson MJ, Kubis H-P. 2011. Taste
1159 perception and implicit attitude toward sweet related to body mass index and soft drink
1160 supplementation. *Appetite* **57**:237–246.
1161 Schuettengruber B, Bourbon H-M, Di Croce L, Cavalli G. 2017. Genome Regulation by
1162 Polycomb and Trithorax: 70 Years and Counting. *Cell* **171**:34–57.
1163 Sen SQ, Chanchani S, Southall TD, Doe CQ. 2019. Neuroblast-specific open chromatin allows
1164 the temporal transcription factor, Hunchback, to bind neuroblast-specific loci. *Elife* **8**.
1165 doi:10.7554/eLife.44036
1166 Shannon CE. 1948. A mathematical theory of communication. *The Bell System Technical*
1167 *Journal* **27**:379–423.
1168 Shen L, Sinai M. 2013. GeneOverlap: Test and visualize gene overlaps. *R package version*
1169 **1**:2013.
1170 Shiraiwa T, Carlson JR. 2007. Proboscis extension response (PER) assay in Drosophila. *J Vis*
1171 *Exp* 193.
1172 Slack C, Alic N, Foley A, Cabecinha M, Hoddinott MP, Partridge L. 2015. The Ras-Erk-ETS-
1173 Signaling Pathway Is a Drug Target for Longevity. *Cell* **162**:72–83.
1174 Smith JM. 2000. The Concept of Information in Biology. *Philos Sci* **67**:177–194.
1175 Su C, Schwarz TL. 2017. O-GlcNAc Transferase Is Essential for Sensory Neuron Survival and
1176 Maintenance. *J Neurosci* **37**:2125–2136.

1177 Sui B, Chen D, Liu W, Wu Q, Tian B, Li Y, Hou J, Liu S, Xie J, Jiang H, Luo Z, Lv L, Huang F, Li
1178 R, Zhang C, Tian Y, Cui M, Zhou M, Chen H, Fu ZF, Zhang Y, Zhao L. 2020. A novel
1179 antiviral lncRNA, EDAL, shields a T309 O-GlcNAcylation site to promote EZH2 lysosomal
1180 degradation. *Genome Biol* **21**:228.
1181 Sung H, Vesela I, Driks H, Ferrario CR, Mistretta CM, Bradley RM, Dus M. 2022. High-sucrose
1182 diet exposure is associated with selective and reversible alterations in the rat peripheral
1183 taste system. *Curr Biol*. doi:10.1016/j.cub.2022.07.063
1184 Szklarczyk D, Gable AL, Nastou KC, Lyon D, Kirsch R, Pyysalo S, Doncheva NT, Legeay M,
1185 Fang T, Bork P, Jensen LJ, von Mering C. 2020. The STRING database in 2021:
1186 customizable protein–protein networks, and functional characterization of user-uploaded
1187 gene/measurement sets. *Nucleic Acids Res* **49**:D605–D612.
1188 Thomas GM, Huganir RL. 2004. MAPK cascade signalling and synaptic plasticity. *Nat Rev*
1189 *Neurosci* **5**:173–183.
1190 van Steensel B, Henikoff S. 2000. Identification of in vivo DNA targets of chromatin proteins
1191 using tethered dam methyltransferase. *Nat Biotechnol* **18**:424–428.
1192 Vaziri A, Dus M. 2021. Brain on food: The neuroepigenetics of nutrition. *Neurochem Int*
1193 **149**:105099.
1194 Vaziri A, Khabiri M, Genaw BT, May CE, Freddolino PL, Dus M. 2020. Persistent epigenetic
1195 reprogramming of sweet taste by diet. *Sci Adv* **6**. doi:10.1126/sciadv.abc8492
1196 Vella P, Scelfo A, Jammula S, Chiacchiera F, Williams K, Cuomo A, Roberto A, Christensen J,
1197 Bonaldi T, Helin K, Pasini D. 2013. Tet proteins connect the O-linked N-acetylglucosamine
1198 transferase Ogt to chromatin in embryonic stem cells. *Mol Cell* **49**:645–656.
1199 Wang J, Liu R, Hawkins M, Barzilai N, Rossetti L. 1998. A nutrient-sensing pathway regulates
1200 leptin gene expression in muscle and fat. *Nature* **393**:684–688.
1201 Wang Q-P, Lin YQ, Lai M-L, Su Z, Oyston LJ, Clark T, Park SJ, Khuong TM, Lau M-T, Shenton
1202 V, Shi Y-C, James DE, Ja WW, Herzog H, Simpson SJ, Neely GG. 2020. PGC1α Controls
1203 Sucrose Taste Sensitization in Drosophila. *Cell Rep* **31**:107480.
1204 Weirauch MT, Yang A, Albu M, Cote AG, Montenegro-Montero A, Drewe P, Najafabadi HS,
1205 Lambert SA, Mann I, Cook K, Zheng H, Goity A, van Bakel H, Lozano J-C, Galli M, Lewsey
1206 MG, Huang E, Mukherjee T, Chen X, Reece-Hoyes JS, Govindarajan S, Shaulsky G,
1207 Walhout AJM, Bouget F-Y, Ratsch G, Larrondo LF, Ecker JR, Hughes TR. 2014.
1208 Determination and inference of eukaryotic transcription factor sequence specificity. *Cell*
1209 **158**:1431–1443.
1210 Weiss M, Anderluh M, Gobec M. 2021. Inhibition of O-GlcNAc Transferase Alters the

1211 Differentiation and Maturation Process of Human Monocyte Derived Dendritic Cells. *Cells*
1212 **10**. doi:10.3390/cells10123312
1213 Wilinski D, Winzeler J, Duren W, Persons JL, Holme KJ, Mosquera J, Khabiri M, Kinchen JM,
1214 Freddolino PL, Karnovsky A, Dus M. 2019. Rapid metabolic shifts occur during the
1215 transition between hunger and satiety in Drosophila melanogaster. *Nat Commun* **10**:4052.
1216 Wise PM, Nattress L, Flammer LJ, Beauchamp GK. 2016. Reduced dietary intake of simple
1217 sugars alters perceived sweet taste intensity but not perceived pleasantness. *Am J Clin*
1218 *Nutr* **103**:50–60.
1219 You Z, Peng D, Cao Y, Zhu Y, Yin J, Zhang G, Peng X. 2021. P53 suppresses the progression
1220 of hepatocellular carcinoma via miR-15a by decreasing OGT expression and EZH2
1221 stabilization. *J Cell Mol Med* **25**:9168–9182.
1222 Zhang X, Ma L, Qi J, Shan H, Yu W, Gu Y. 2015. MAPK/ERK signaling pathway-induced hyper-
1223 O-GlcNAcylation enhances cancer malignancy. *Mol Cell Biochem* **410**:101–110.